NRL Memorandum Report 3217

DARPA-NRL Laser Program Semiannual Technical Report to Advanced Research Projects Agency

1 January 1975 to 30 June 1975

Laser Physics Branch
Optical Sciences Division

February 1976

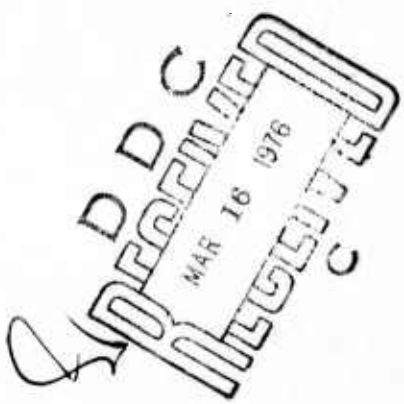

NAVAL RESEARCH LABORATORY
Washington, D.C.

SECURITY CLASSIFICATION OF THIS PAGE (When Data Entered)

REPORT DOCUMENTATION PAGE

READ INSTRUCTIONS BEFORE COMPLETING FORM

1. REPORT NUMBER: NRL ~~Memorandum~~ ~~Report~~ -3217
2. GOVT ACCESSION NO.
3. RECIPIENT'S CATALOG NUMBER
4. TITLE (and Subtitle): DARPA-NRL LASER PROGRAM - SEMIANNUAL TECHNICAL REPORT TO DEFENSE ADVANCED RESEARCH PROJECTS AGENCY, ~~1 JANUARY 1975 TO 30 JUNE 1975~~
5. TYPE OF REPORT & PERIOD COVERED: Interim report on continuing NRL Problems
6. PERFORMING ORG. REPORT NUMBER
7. AUTHOR(s): Laser Physics Branch
8. CONTRACT OR GRANT NUMBER(s): ARPA Order-2062
9. PERFORMING ORGANIZATION NAME AND ADDRESS: Naval Research Laboratory, Washington, D.C. 20375
10. PROGRAM ELEMENT, PROJECT, TASK AREA & WORK UNIT NUMBERS: NRL ~~Problems~~ NO1-48 & 49, KO3-53, Project No. 5E20
11. CONTROLLING OFFICE NAME AND ADDRESS: Interim rept. 1 Jan 75 - 30 Jun 75
12. REPORT DATE: February 1976
13. NUMBER OF PAGES: 114
14. MONITORING AGENCY NAME & ADDRESS (if different from Controlling Office): Defense Advanced Research Projects Agency, Arlington, VA 22209
15. SECURITY CLASS. (of this report): UNCLASSIFIED
15a. DECLASSIFICATION/DOWNGRADING SCHEDULE
16. DISTRIBUTION STATEMENT (of this Report): Approved for public release; distribution unlimited
17. DISTRIBUTION STATEMENT (of the abstract entered in Block 20, if different from Report): 113 p.
18. SUPPLEMENTARY NOTES: NRL-NO1-48, NRL-NO1-49
19. KEY WORDS (Continue on reverse side if necessary and identify by block number)

Lasers	Electronic state lasers	Chemiluminescence
Electrical lasers	Chemical kinetics	
Chemical lasers	Electronic state lifetimes	
Laser diagnostics	Energy transfer	

20. ABSTRACT (Continue on reverse side if necessary and identify by block number)

The DARPA-NRL Laser Program is concerned with the development of laser technology in three project areas: chemical infrared lasers, electrical infrared lasers and electronic-state lasers. The chemical infrared laser program includes studies of pulsed HCl laser systems and molecular energy transfer processes. Several chlorinated hydrocarbons have been identified as attractive chlorine sources for HCl lasers
(Continued) OVER

DD FORM 1 JAN 73 1473 EDITION OF 1 NOV 63 IS OBSOLETE S/N 0102-014-6601

SECURITY CLASSIFICATION OF THIS PAGE (When Data Entered)

251950

20. Abstract (Continued)

based on the Cl + HI reaction. Vibrational relaxation rates for the CO laser and the potential D_2^* + HCl V-V transfer laser system have been measured.

The electrical infrared program emphasizes electric-discharge gasdynamic lasers and electron-beam pumping of potential laser systems in the mid infrared. Studies of the D_2^* → HCl system have been continued along with detailed measurements of the discharge and flow characteristics. The D_2^*-CO_2^* laser system previously discovered has been found to have comparable efficiency to the N_2^*-CO_2^* EDGDL.

A number of excitation approaches are being evaluated for application to electronic state lasers. Discovery of the XeBr laser as a result of electron-beam excitation of Xe/Br_2 mixtures has led to the rare-gas halide laser systems. Successful transverse excitation of copper chloride offers promise as a more efficient copper vapor laser. Electrical and optical pumping schemes to extend the range of operation of the previously reported Hg vapor laser are described. Lifetime measurements of the HgBr(B) state have been completed and an estimate made of the lifetime of upper vibrational levels of the HgBr(X) state.

TABLE OF CONTENTS

FOREWORD

The Laser Physics Branch of the Optical Sciences Division, Naval Research Laboratory, Washington, D. C., prepared this semiannual report on work sponsored by the Advanced Research Projects Agency, ARPA Order 2062. Co-authors of the report were J. R. Airey, R. Burnham, L. Champagne, N. Djeu, D. Frankel, J. K. Hancock, N. W. Harris, G. A. Hart, M. C. Lin, T. J. Manuccia, S. K. Searles, J. A. Stregack, W. S. Watt, and B. Wexler.

SEMIANNUAL TECHNICAL REPORT

REPORTING PERIOD

1 Jan 1975 - 30 June 1975

1.	DARPA Order	2062, Amendment No. 3
2.	Program Code Number	5E20
3.	Name of Contractor	Naval Research Laboratory
4.	Effective Date of Contract	1 July 1972
5.	Contract Expiration Date	30 June 1975
6.	Amount of Contract	$550,000
7.	Contract Number	62301E
8.	Principal Investigator	J. R. Airey
9.	Telephone Number	(202) 767-3217
10.	Project Scientist	W. S. Watt
11.	Telephone Number	(202) 767-2074
12.	Title of Work	DARPA/NRL Laser Technology Program

SPONSORED BY

DEFENSE ADVANCED RESEARCH PROJECTS AGENCY

DARPA Order No. 2062

DARPA-NRL LASER PROGRAM
SEMIANNUAL TECHNICAL REPORT TO ADVANCED
RESEARCH PROJECTS AGENCY
1 JANUARY 1975 TO 30 JUNE 1975

CHEMICAL INFRARED LASERS

1. Pulsed HCl Chemical Laser

The aim of the experiments on pulsed HCl lasers is to evaluate the potential of several mixtures of reactants which are capable of being premixed and could lead to improved pulsed HCl laser performance.

Typically pulsed HCl lasers operate using either the H_2/Cl_2 mixture which has the assumed reaction sequence

$$Cl + H_2 \rightarrow HCl + H \qquad -1 \text{ kcal/mole} \qquad (1)$$

$$H + Cl_2 \rightarrow HCl^* + Cl \qquad +45 \text{ kcal/mole} \qquad (2)$$

or the HI/Cl_2 system which operates on the two exothermic reactions

$$H + Cl_2 \rightarrow HCl^* + Cl \qquad +45 \text{ kcal/mole} \qquad (3)$$

$$Cl + HI \rightarrow HCl^* + I \qquad +32 \text{ kcal/mole} \qquad (4)$$

In the H_2/Cl_2 system, endothermic reaction (1) is slow on the time scale of the laser pulse and therefore contributes neither to the production of excited HCl nor to the supply of H atoms for reaction (2). The requisite H atoms must come directly from the dissociation of H_2 in the discharge. HI is a better source of atomic hydrogen than H_2 and one would expect the HI/Cl_2 system to be more efficient.

Note: Manuscript submitted January 29, 1976.

However, premixing of HI and Cl_2 is difficult to perform without spontaneous reaction which not only depletes the fuel but also creates ground state HCl. Alternate chlorine sources, R-Cl, are being sought which are sufficiently reactive so that the resulting HI/R-Cl mixture will out-perform the H_2/Cl_2 system and in addition can be premixed with HI without significant prereaction.

The laser used in this present study uses a transverse electrical pin discharge to initiate the reaction between R-Cl and HI and was described previously[1]. During the present reporting period screening experiments were continued in order to evaluate the performance of R-Cl/HI mixtures against the baseline H_2/Cl_2 system.

These screening experiments have been completed and the results described in a paper accepted for publication[2] (see Appendix A). The major conclusions are that several chlorinated hydrocarbons are attractive chlorine sources both in terms of laser output and specific output when compared with H_2/Cl_2 mixtures.

During the next reporting period some of these improved cavity fuels will be evaluated using an e-beam sustainer for initiation of the chemical reactions leading to the HCl laser.

References

1. NRL ARPA Semiannual Report, 1 July - 31 December 1974, NRL Memorandum Report No. 3084.

2. T. J. Manuccia, J. A. Stregack and W. S. Watt, IEEE J. Qu. E. QE 11, 921, (1975).

2. Carbon Monoxide Energy Transfer Studies

Measurements of energy transfer rates in CO under ARPA sponsorship have provided much kinetic data relevant to CO and CO_2 lasers. Additionally, previously reported vibration to vibration (V→V) rate studies in CO-additive mixtures predicted the recently discovered V→V transfer lasers $CO-CS_2$, CO-OCS and $CO-N_2O$. The goals of this program during the current reporting period are two fold:

Provide vibration to translation (V→T) quenching rates for CO in the presence of low molecular weight diluent gases and

Measure the D_2 self relaxation rate as a function of temperature to provide kinetic rate data for the D_2-HCl V→V transfer laser understudy at NRL.

Because of the potentially large temperature range which must be considered in the CO and D_2-HCl laser devices, the present investigation covered the unusually large range of $110^{\circ}K$-$630^{\circ}K$. All rates reported were strongly temperature dependent with some deactivation probabilities increasing an order of magnitude for a $100^{\circ}K$ change in temperature.

a. CO Quenching Rates by Low Molecular Weight Diluent Gases

The first objective of this program is to study CO(v=1) deactivation characteristics by the light collision partners, H_2, HD, D_2, and He. Excitation of CO ground state molecules to the CO(v=1) state was accomplished using the selective excitation of a frequency doubled CO_2 laser. Quenching of CO(v=1) occurs through the following V→T pathway:

$$CO(v=1) + H_2 \xrightarrow{k_{CO-H_2}} CO(v=0) + H_2 + \Delta E = 2143\ cm^{-1} \quad (1)$$

$$CO(v=1) + HD \xrightarrow{k_{CO-HD}} CO(v=0) + H_2 + \Delta E = 2143\ cm^{-1} \quad (2)$$

$$CO(v=1) + D_2 \xrightarrow{k_{CO-D_2}} CO(v=0) + H_2 + \Delta E = 2143\ cm^{-1} \quad (3)$$

$$CO(v=1) + He \xrightarrow{k_{CO-He}} CO(v=0) + H_2 + \Delta E = 2143\ cm^{-1} \quad (4)$$

Since the molecular weight of the collision partner studied in Equation (1) - (4) ranges from 2-4, one would not expect to see significant differences between these additive species. As shown in Figure 1, however, H_2 is at least a factor of ten more efficient in deactivating CO than D_2. Additionally CO(v=1) quenching by HD falls close to the $CO-H_2$ results, rather than half way between H_2 and D_2 as would be expected by the difference in molecular weights. The following conclusions can be reached from these measurements:

(1) The probability of deactivation of CO(v=1) by D_2 and He is identical over the temperature range studied. This is strong evidence for a Landau-Teller type deactivation mechanism, i.e., rotational energy levels in D_2 do not participate in the quenching mechanism.

(2) The probability of deactivation of CO(v=1) by H_2 is much greater than CO-D_2. A mass effect alone is insufficient to explain this difference. Apparently vibrational to rotational (V→R) energy transfer is occurring via processes of the type

$$CO(v=1)+H_2(v=0,j=2) \rightarrow CO(v=0)+H_2(v=0,j=6)+\Delta E = 88cm^{-1} \quad (5)$$

(3) At temperatures near 100°K, the deactivation probability for CO(v=1) is only one in every 10^9 collisions with D_2 or He. For CO-H_2 and CO-HD collisions this probability is 10^{-7} -10^{-8}. Consequently, high pressures of the above diluent gases should have minimal poisoning effect on CO laser performance at low temperatures.

b. D_2(v=1) Quenching Rates by D_2 and CO

One possible disadvantage in using D_2 as a diluent gas in CO lasers is the endothermic transfer process:

$$CO(v=1) + D_2(v=0) \underset{k_e^1}{\overset{k_e}{\rightleftarrows}} CO(v=0) + D_2(v=1) + \Delta E = -850cm^{-1} \quad (6)$$

Once the species D_2(v=1) is produced, efficient relaxation might be expected to occur via the process

$$D_2(v=1)+D_2(v=0) \xrightarrow{k_{D_2-D_2}} D_2(v=0)+D_2(v=0)+\Delta E\ 2993cm^{-1} \quad (7)$$

We have measured rate constants k_e and $k_{D_2-D_2}$ shown in Equation (6) and (7) through use of the double exponential decay curve analysis discussed in previous reports. The reverse rate in Equation (6), k_e^1, can be determined using $k_e^1 = k_e \exp(-\Delta E/kT)$. These results are shown in Figure 2. Because V→V transfer into the $D_2(v=1)$ level via equation (6) is faster than V→R,T deactivation out via equation (7), a steady state concentration of excited D_2 molecules is established. Quenching measurements for the $D_2(v=1)$ level are possible because the fluorescence decay of $CO(v=1)$ is kinetically linked to the $D_2(v=1)$ level, resulting in the observation of two fluorescence lifetimes.

The present experimental study of the rate constants k_{CO-H_2}, k_{CO-H_2}, k_{CO-HD}, k_{CO-He}, k_e^1, and $k_{D_2-D_2}$, differs from previous studies which were predominately concerned with near resonant V→V energy transfer. As shown in equations (1) - (7), large amounts of energy must be transferred into the translational degrees of freedom of the gas mixture during an inelastic collision process. Consequently, we see steep temperature dependencies with rates increasing with temperature. A clear example of this can be seen in

Figure 2 for the D_2 self quenching probability. Over the temperature range 150-500°K, an increase of three orders of magnitude for this process is indicated.

These data are described in greater detail in one recently published paper [1] and in another accepted for publication [2]

References

1. D. F. Starr and J. K. Hancock, J. Chem. Phys. 62, 3747 (1975).

2. D. F. Starr and J. K. Hancock, J. Chem. Phys. (to be published, December, 1975).

3. Polyatomic Energy Transfer

The primary goal of the project is to measure intramolecular vibration to vibration (V→V) energy transfer rates in several polyatomic molecules, beginning with SF_6 and BCl_3. These molecules are chosen because they are known to be strong absorbers of CO_2 laser radiation.

Although the vibration to translation (V→T) energy transfer rates of many polyatomic molecules have been measured, the much more rapid intramolecular V→V energy transfer rates have not been determined because no suitable high power, short-pulse laser source was available. The development of a high energy, one nanosecond CO_2 laser system at NRL under DARPA sponsorship permits the measurement of intramolecular V→V energy transfer rates of many polyatomic

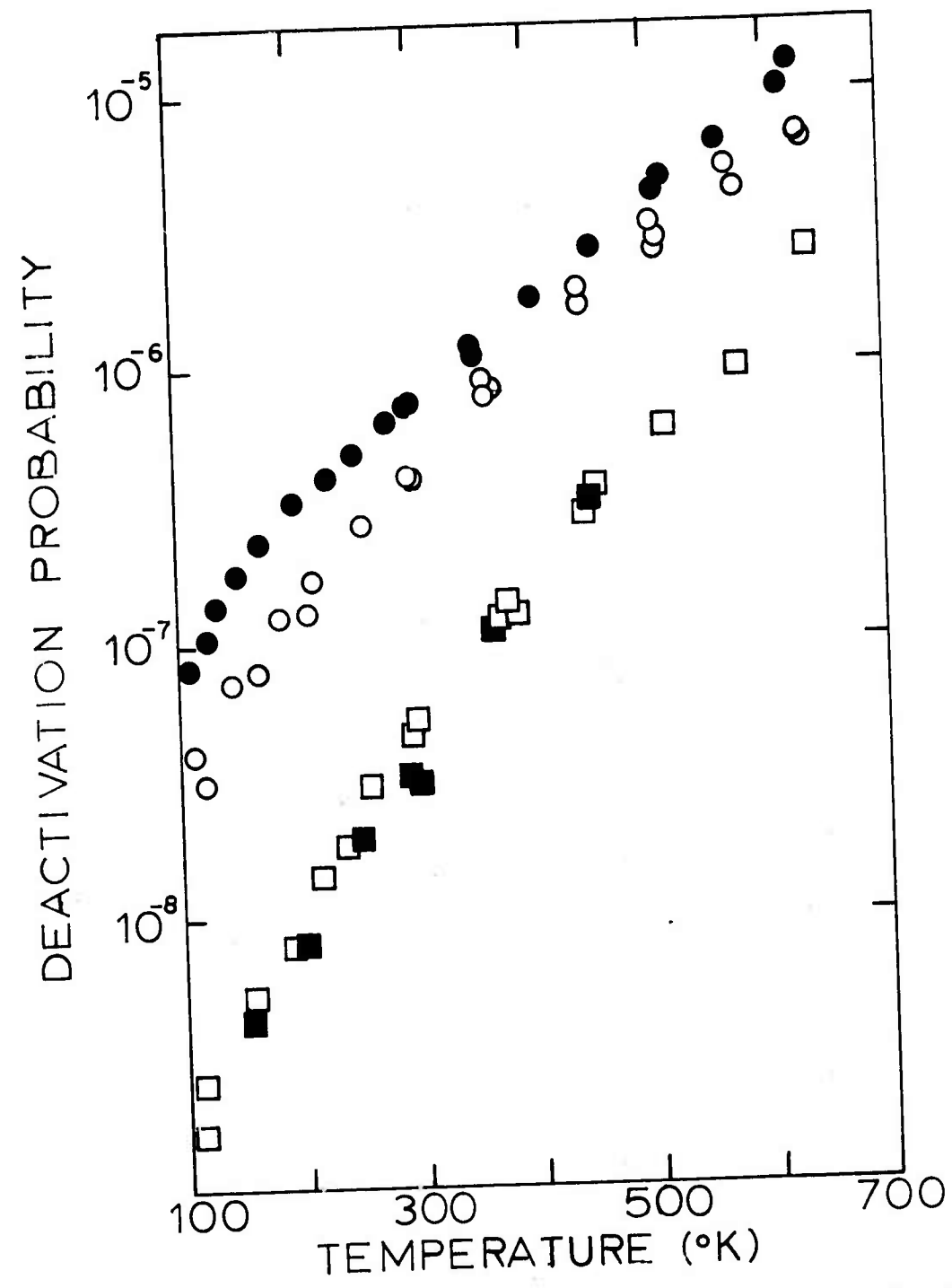

Fig. 1 - Deactivation probability of CO(v=1) in collisions with H_2, HD, D_2, and He over the temperature range 110-630°K. Data points shown are CO-H_2 ●; CO-HD ○; CO-D_2 ■; and CO-He □.

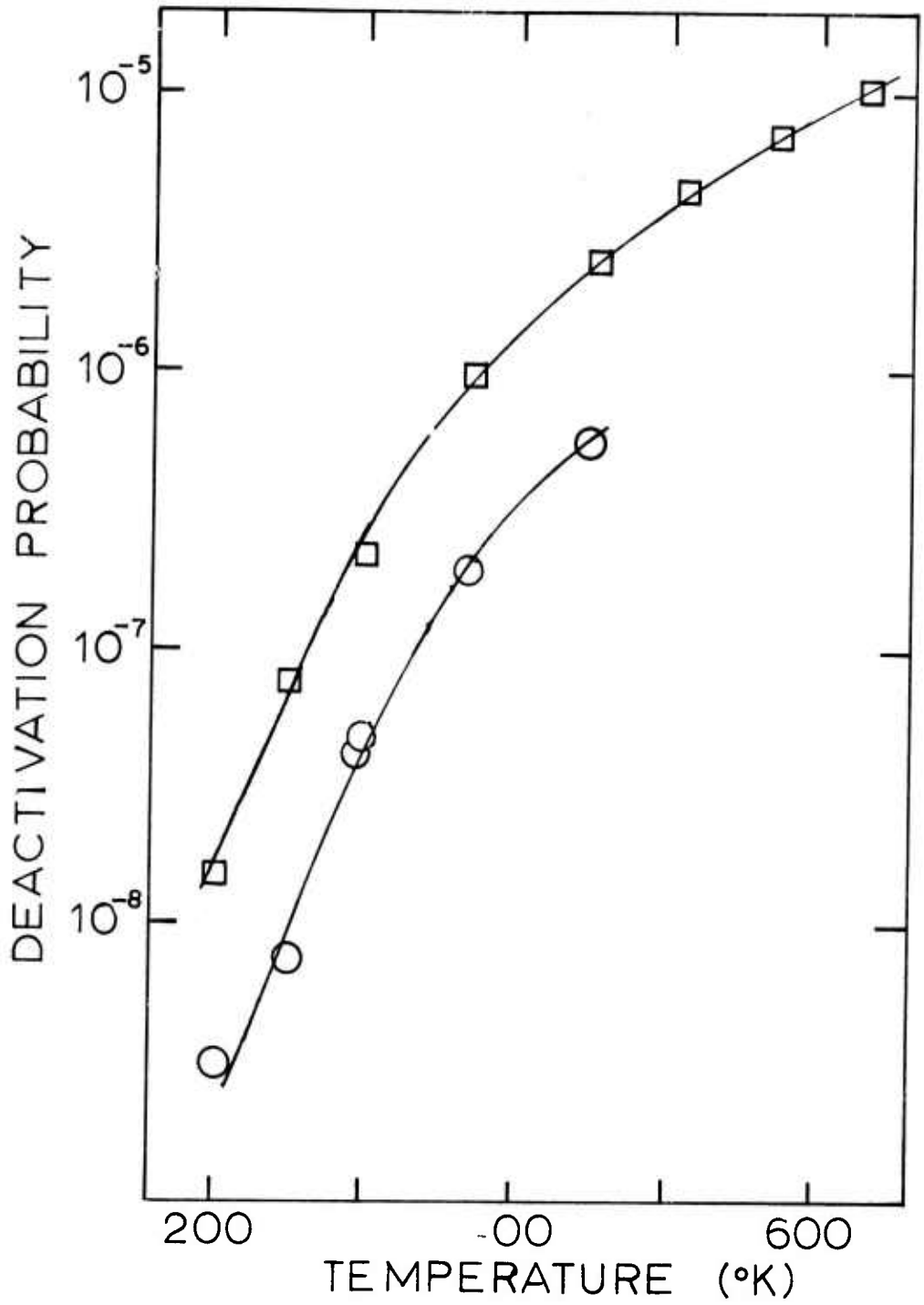

Fig. 2 - Deactivation probability versus temperature for the following kinetic processes:

$D_2(v=1) + CO(v=0) \rightleftarrows D_2(v=0) + CO(v=1) + \Delta E = 850\ cm^{-1}$

$D_2(v=1) + D_2(v=0) \rightarrow 2D_2(v=0) + \Delta E = 2993\ cm^{-1}$

Data points are D_2-CO □ ; D_2-D_2 ○.

molecules. Such measurements represent not only an advance in the state of knowledge of energy transfer, but also have the immediate practical result of determining which if any of these molecules can be used as an optical isolator in high power CO_2 laser amplifier chains.

A description of the double-resonance method employed and a diagram of the apparatus were included in the previous report. Several improvements in the apparatus have been made since that time. A recently obtained half-wave etalon of cadmium sulfide has been doubly useful. Because it produces a rotation in the plane of polarization of a CO_2 laser beam, it can be placed between the cw monitoring laser and the germanium plate attenuator to continuously control the power delivered to the sample cell without disturbing the alignment. This is particularly advantageous when trying to find an optimum trade-off between maximum signal level and minimum perturbation of the levels being monitored. The same etalon has been used to facilitate alignment of the nanosecond laser beam through the sample cell. Placed between the Pockels cell and the analyzer stack, a 90° change in polarization is produced, permitting the entire laser pulse train to pass through the analyzer stack unattenuated and undeflected. Rotation of the analyzer stack by 90° would also permit the beam to pass through, but would also produce a large angular deflection. The

etalon is of course removed when the experiment is to be done.

A new stainless steel sample cell was constructed, replacing the original glass and teflon design. Having all welded joints and "O" rings only where the windows are held, it decreased the outgassing and leak rate of the sample system. A new capacitance manometer head with a 1000 torr range was added to the 10 torr head already in place to adequately cover the pressure range of interest without recourse to a mercury manometer-cathetometer combination. This change improves accuracy in addition to avoiding contact of mercury with corrosive gases such as BCl_3.

An electronic amplifier already available in the lab was tested for suitability in these experiments. Its measured 5 ns risetime was considered adequate for the initial phase of the work, but its 15% overshoot and ringing were too great to be useful. The manufacturer was able to reduce this to 6%, which is satisfactory for present operating conditions. Higher quality amplifiers are now on order.

Preliminary double resonance experiments were successfully attempted using the entire mode locked pulse train. This assured that beam and detector positioning were correct. Similar experiments were also performed using the six most intense pulses in the train.

Single pulse experiments are now underway. In 150 mtorr of SF_6, an exponential risetime constant of $\sim$ 60 ns was observed with $\sim$ 30 torr of added helium, and 30 ns with 75 torr of helium. Limited signal-to-noise ratio precludes quoting these numbers with greater precision. Considerable effort is now being directed toward reducing the noise and toward finding a suitable method of signal averaging.

One other significant activity occurred during the reporting period. This was a test of the risetime of a new infrared detector material. The detector being used now has a risetime constant of 17 ns and a falltime constant of 46 ns. The manufacturer claimed to have a high speed material with a 1 ns time constant. A sample detector was shipped to us and tested using the Pockels cell as a high speed "gate". The new sample was found to have the same time constant as the ordinary material and has been rejected and returned to the manufacturer. Thus the single nanosecond CO_2 pulse generating system provides an easy check of the reliability of manufacturers' claims for detector response times.

ELECTRICAL INFRARED LASERS

1. Electric Discharge Gasdynamic Lasers

In the Electric Discharge Gasdynamic Laser (EDGDL) facility, experiments are aimed at producing new and efficient cw electrical lasers. Primary interest is in the 3-5 micron region. Since the candidate laser molecules have not been successfully excited by direct electron impact, attempts are being made at producing laser systems by energy transfer from deuterium or hydrogen excited in an electric discharge.

A description of the EDGDL facility has been given in previous reports [1-3]. During this period, experiments were performed to characterize the operation of the EDGDL at plenum pressures up to 150 torr and to obtain data for comparison with computer model predictions. The modelling is being performed by Physical Sciences Inc. of Wakefield, Mass. under a contract funded by both the Navy and ARPA and will be used to predict the optimum operating conditions for the proposed D_2-HCl laser.

The subsonic discharge plenum region was characterized for several D_2-He mixtures with the maximum amount of D_2 being 42% by volume. For each of these mixtures the PSI discharge model predicted that over 70% of the electrical energy would be deposited in the vibrational mode of D_2 for

the E/N of these experiments ($\sim$ 1 x 10^{-16} volts cm^2). The experimental E/N has not been corrected for the voltage drop in the cathode fall region of the discharge which can be appreciable and therefore the self-sustained glow discharge operates at less than optimum E/N for vibrational excitation. However, from an energy balance based on the energy deposited in the gas and the pressure rise (and hence temperature rise) when the discharge is turned on it has been estimated that approximately 65% of the electrical energy is deposited in the vibrational mode of D_2. For Ar-D_2 mixtures it was found to be more difficult to maintain a stable arc-free glow discharge. Good discharges could only be maintained at low current (less than 10 ma) and power loadings when the dc discharge had either rf augmentation or a large choke was used as an arc suppressor.

Following characterization of the discharge, the effect of varying the injection of the lasing species on the supersonic gasdynamics was investigated. At these higher plenum pressures it was observed that there is a critical secondary flow rate below which supersonic flow is maintained throughout the cavity region. Higher flow rates cause the cavity pressure to increase sharply. The sharp pressure increase is the effect of shock waves "choking" the flow due to excessive secondary mass addition. A typical curve of cavity pressure vs. secondary flow rate is

shown in Figure 3. It has been experimentally determined that the percentage of secondary flow which induces choking increases as the plenum pressure and/or molecular weight of the primary flow is increased. For the mixtures tested this percentage was 1.5% for He-D_2 mixtures and 10% for Ar-D_2 mixtures.

In order to determine the effects of the cavity gas-dynamics upon the D_2-HCl energy transfer system, HCl fluorescence traces were taken over the entire length of the cavity for choked and unchoked conditions. Figure 4 shows characteristic traces for both choked and unchoked conditions. For the choked condition the fluoresence peaks halfway through the cavity region and then decreases as deactivation becomes important because of the decelerated flow. For the unchoked cavity the fluorescence increases until approximately 19 cm where it then levels off. Using a series of bandpass filters, the relative spectral intensity distribution of the HCl fluoresence taken for the unchoked case is

filter	detector signal
3.2 → 3.9	2.5 mV
> 4.1 μ	.03 mV
> 3.8 μ	.15 mV

The signal observed using the last two filters could come from either high rotational levels of the lower vibrational

states or from the lower rotational levels of the higher vibrational states.

Information about these two possibilities is gained indirectly from gain measurements of the N_2-CO_2 and D_2-CO_2 laser systems operating in the same facility. From these gain measurements as a function of J, T_v and T_r were extracted. For the N_2-CO_2 system there is little variation in T_v and T_r as a function of position downstream of the nozzle exit plane. Typically the rotational temperature for the unchoked cases were under 200°K while for the choked cases the rotational temperatures were over 200°K. For the D_2-CO_2 system, the variation in vibrational and rotational temperature as a function of distance from the nozzle exit plane is shown in Figure 5 for both the choked and unchoked cavity flows operating from the same plenum conditions. Excluding the temperatures measured at the position 12.1 cm downstream from the nozzle exit plane the general shape of the variation of T_v is similar to the HCl fluorescence traces. Comparing the rotational temperatures, the choked case starts out higher, but both cases reach a final temperature which is considerably higher than in the unchoked N_2-CO_2 case. This is caused both by the vibrational energy difference between D_2 and $CO_2(001)$ being converted into translational/rotational energy and by the supersonic heat addition which takes place as a result of this temperature rise.

As a result of these gain measurements it would appear that in the unchoked case the HCl fluorescence above 3.8 μ comes from the lower rotational lines of higher ($v \geq 3$) HCl vibrational levels. One is also lead to the conclusion that the lower plenum pressure runs made in previous reporting periods were made under choked (i.e. high rotational temperature) conditions. This would practically explain the failure to develop a CS_2 laser since the lower laser level is only 657 cm^{-1} above the ground state and thus would be thermally populated. The increased temperature is less important in a D_2-CO_2 laser system but would alter the rotational distribution in the D_2-HCl system reducing any partial inversion.

Present plans call for further study of the D_2-HCl system in order to validate the computer model before using it to predict the conditions under which lasing will occur. As a result of the studies of the gasdynamics of the EDGDL system it appears to be desirable to use Argon diluent if a stable glow discharge can be maintained or to increase the plenum pressure in order to increase the amount of secondary flow which can be added without choking. In order to accomplish the former, attempts will be made to produce stable glow discharges in Ar-D_2 or Ar-He-D_2 plenum mixtures while in order to increase the plenum pressure, the e-beam sustainer system will be completed and a new nozzle array

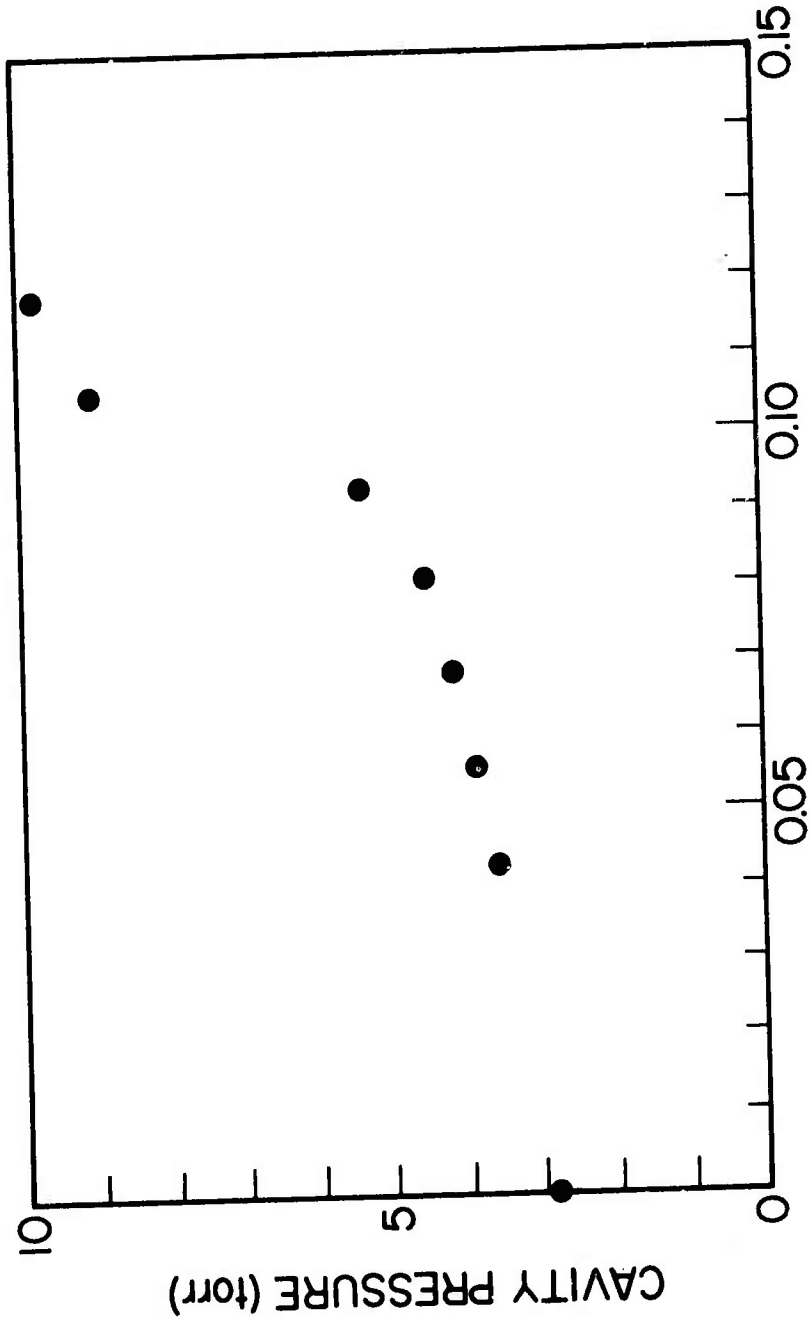

Fig. 3 - Effect of secondary flow addition on cavity pressure

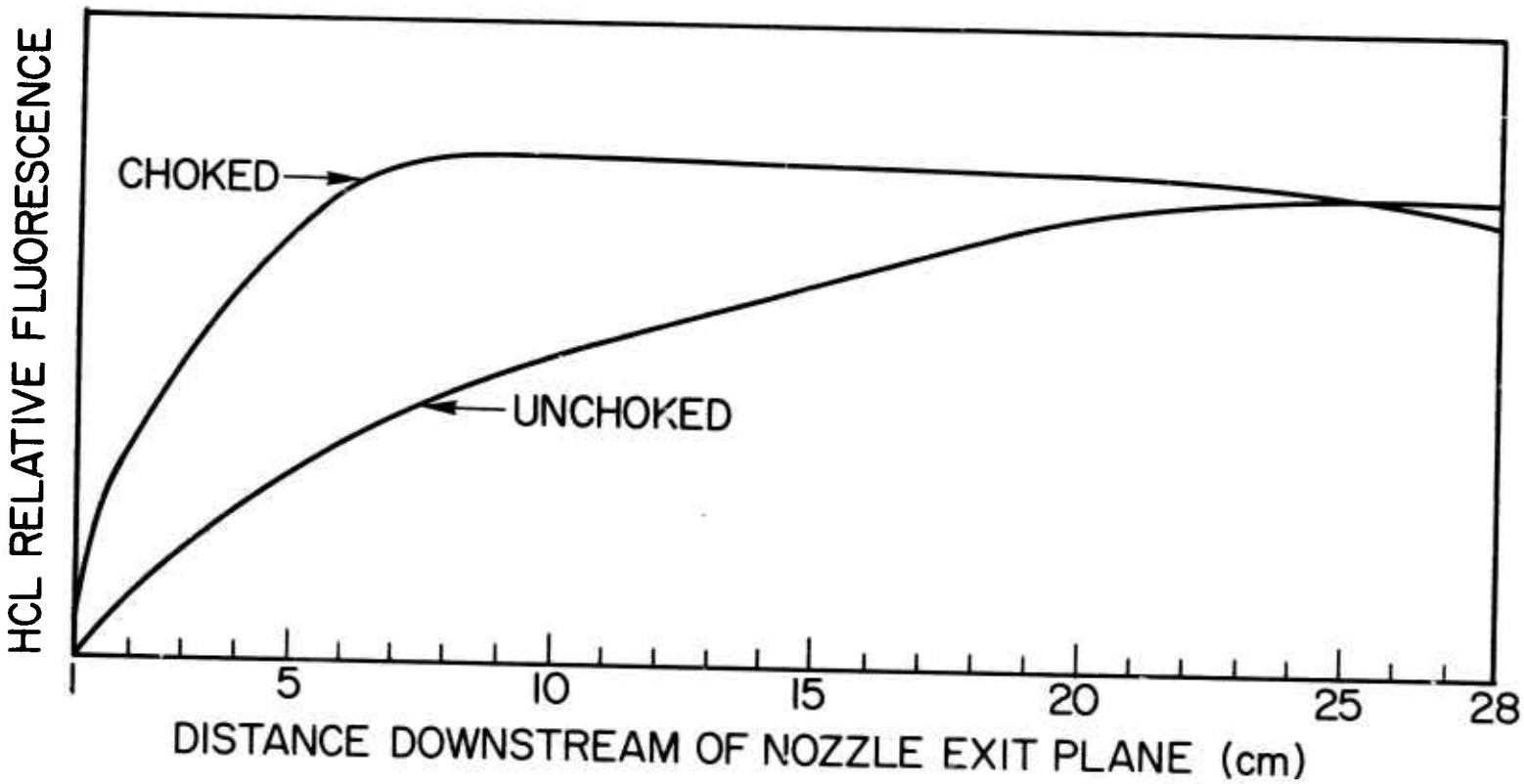

Fig. 4 - HCl fluorescence vs distance from the nozzle exit plane for both choked and unchoked flow conditions

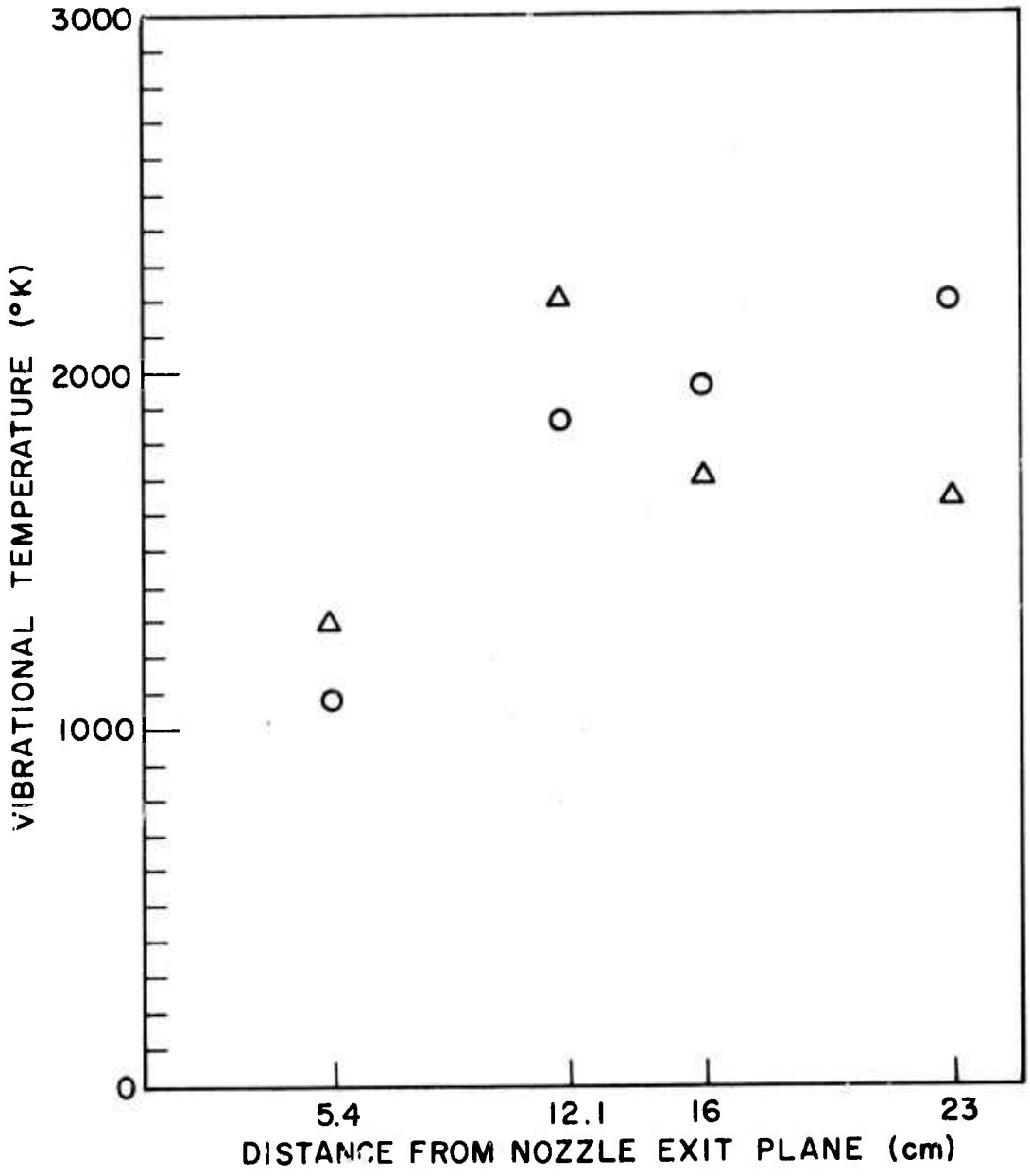

Fig. 5 - CO_2 ($00^0 1$) vibrational temperature vs distance from the nozzle exit plane for CO_2 excited via energy transfer from D_2 for both (△) choked and (○) unchoked flow conditions.

built which will provide cleaner g. dynamics without impairing the mixing. With the ability to supersonically mix the secondary while maintaining low rotational temperatures, lasing will be attempted from CO-CS_2 as well as from N_2O and C_2H_2 via transfer from CO, H_2 and/or D_2.

References

1. NRL-ARPA Laser Program Semiannual Technical Report, 1 July-31 December 1973, NRL Memorandum Report 2846.

2. NRL-ARPA Laser Program Semiannual Technical Report, 1 January-30 June 1974, NRL Memorandum Report 3005.

3. NRL-ARPA Laser Program Semiannual Technical Report, 1 July-31 December 1974, NRL Memorandum Report 3084.

2. E-Beam Sustainer Pumped HCl Laser

The objective of the pulsed electrical laser program for this reporting period was to determine the experimental parameters which most favor stimulated emission for HCl-diluent mixtures and to establish the influence of these parameters on the critical processes which are involved in producing a partial population inversion between HCl vibrational levels. These experimental parameters include the sustainer voltage, e-beam voltage, and e-beam cathode to foil distance of the cold cathode e-beam sustainer discharge system, as well as the partial pressures of HCl and various diluents used as gas mixtures.

2.1 HCl Fluorescence Measurements

a. Objective

Fluorescence measurements were taken to establish the effect of these parameters on a number of simultaneously occurring critical

processes. These processes are HCl vibrational excitation by direct electron impact, HCl self-deactivation, HCl dissociation, and gas heating by the discharge. The extent to which it is possible to channel the available discharge energy into vibrational excitation of HCl will determine if a partial inversion can be produced between HCl vibrational levels and will also establish the maximum possible efficiency of any resulting HCl laser. In choosing the appropriate discharge E/N value, HCl self-deactivation will limit the HCl partial pressure. Atomic products of HCl dissociation must be minimized since they serve as highly effective quenchers of vibrationally excited HCl. The degree of gas heating by the discharge is important because of several considerations. First, gas heating represents an energy loss which decreases the fractional power transfer to HCl vibrational excitation and hence decreases the overall efficiency of the system, assuming that laser action is not totally prevented by this gas heating. Also, anharmonic vibrational pumping of HCl(v=1) into higher vibrational levels which is required for the operation of the proposed electric discharge HCl laser is severely hampered by any increase in translational temperature. In addition, since only a partial population inversion will be produced, the resulting P-branch gain will be a sensitive function of rotational temperature. To reduce the degrading effect of these highly temperature dependent processes the complex cooling arrangement was constructed and tested on the present e-beam sustainer cavity region.

b. Application to Discharge Kinetics

The contribution of the various kinetic processes were to be analyzed by using time resolved fluorescence measurements of the 3-5 micron region, divided into segments through the use of filters, as input data to an analytical model of the e-beam sustained discharge HCl system being developed in conjunction with Physical Sciences Incorporated (PSI). The analytical treatment can be best understood in terms of its two major components: a theoretical model of the discharge kinetics using available electrical-excitation cross-section data in a computer code solution of the Boltzman equation; and a chemical kinetics model of the subsequent vibrational energy transfer and relaxation reactions. The temporal behavior of the fluorescence observed in the first 2-microseconds during the e-gun pulse serves as a sensitive monitor of the most crucial process of the discharge kinetics, the HCl vibrational excitation. The data gathered at a selected set of experimental conditions, can then be used with the observed time dependence of the sustainer voltage, V_s, sustainer current I_s, and e-gun voltage and current through the foil to achieve agreement between the Boltzmann code predictions and experimental results by making slight modifications in some of the less well known cross-sections used. The resulting cross-section set can then be used to rapidly search for discharge conditions and

gas mixture compositions that will optimize HCl vibrational excitation, thereby eliminating the need to conduct time-consuming scans of the multi-dimensional parameter space spanned by the experimental variables.

c. Application to Inversion Kinetics

Similarly the long fluorescence tail persisting after the discharge terminates can be compared with predictions of an anharmonic-oscillator kinetics code. Once good agreement for the initial set of gas mixtures is achieved, this code can be used in conjunction with the discharge code to determine the experimental conditions which maximize the fractional power transfer to HCl vibrational excitation, subject to the constraint of simultaneously maximizing anharmonic pumping of HCl with minimal loss due to collisional deactivation by HCl, H and Cl.

d. Gas Mixtures Investigated

The required fluorescence measurements were first carried out for Ar-HCl mixtures since rapid electron attachment by HCl makes it impossible to sustain a stable discharge in pure HCl with the NRL device. Furthermore it was initially planned that Ar/HCl or Ar/D_2/HCl mixtures would be used for the actual attempts to produce stimulated emission. Hence, such data was necessary as a test of the discharge code used to model gas mixtures of interest. At the same time use of Ar/HCl data would avoid the discharge and

subsequent chemical kinetics complications that three-component $Ar/D_2/HCl$ mixtures would introduce.

e. Experimental Apparatus

A schematic of the experimental set up used to monitor the HCl fluorescence is shown in Figure 6. A Spectronics Model SD 8720 1 mm diameter indium antimonide photovoltaic detector (In:Sb(PV)), modified to operate in the zero bias mode, was used to provide the highest possible detectivity. The detector was placed at the 12.5 cm focal length of a 2.5 cm diameter KRS5 lens to improve collection efficiency. The In:Sb(PV) detector was r.f. shielded from noise produced by the electron gun and lead shielded from x-rays. Blocking filters were used to select the wavelength region of interest. Signals from the detector were displayed on a Tektronix Model 565 oscilloscope equipped with a Model 1A7A differential amplifier. An absorber cell extended from the end of the discharge region to the output window of the sustainer chamber. This was installed for two purposes. First, HCl self-absorption constitutes a serious problem, and it is essential to minimize such self-trapping wherever possible. By evacuating the absorber cell and then filling it with pure argon any self-trapping in this region could be eliminated. The second use of such a cell was in determining what fraction of fluorescence in the 3-4 micron region was due to HCl (v=1) emission. This could be

accomplished by filling the cell with a 300 torr HCl/300 torr Ar mixture to absorb the HCl (v=1) fluorescence.

f. HCl Self-Absorption

Total pressures of one atmosphere were used to minimize any leakage problems encountered in the system which was employed in a static fill rather than flowing gas mode since cooling of the gas was unnecessary in these Ar/HCl preliminary experiments. The relative concentration of HCl was limited to 0.01% to 1% so that self-trapping would not severely attenuate the HCl emission. As is shown in Figure (7)[1] only the 0.01% mixtures can be correctly considered to be optically thin.

For this relative concentration in a one atmosphere mix the effective self-absorption length should be 50 cm. Thus self-trapping, although still somewhat important, would not totally absorb v=1 to v=0 radiation. As shown in Figure 8 the fluorescence traces display unusual temporal behavior. As the e-gun is crowbarred and the current begins to decay, the 3-4 micron emission shown in Figure 8a triples in intensity and then undergoes a rapid decay with a lifetime of about 1.6 μsec. Since the HCl partial pressure is only 0.001 atmosphere the expected HCl fluoresnce decay time would be approximately 1.6×10^4 μsec. This extremely short decay time observed tends to indicate that argon rather than HCl dominates the fluorescence, and that measurements taken

with low HCl partial pressures to avoid self-trapping problems are incapable of providing needed HCl population data.

g. Argon Infrared Emission

The inference that the observed fluorescence was primarily due to argon was lent further support by the results of filling the absorber cell with a 300 torr HCl/300 torr Ar mixture. As is shown in Figure 8b the 3-4 micron radiation is only attenuated by 22%, a surprisingly low value if HCl is presumed to be the source of emission. Because these data indicated that an Ar 3-4 micron emission problem existed, fluorescence from pure Ar excited by the e-gun alone, and by the e-gun sustainer combustion was studied. The results are shown in Figure 9-11. Figure 9b indicates that emission from pure argon is attenuated by 18% in passing through the absorber cell filled with the same 300 torr HCl/300 torr Ar mixture. These attenuation results are listed in Table I. This 18% attenuation value is close enough to the 22% figure measured for the 0.01% mixture to strongly suggest that Ar, rather than HCl, emission was being observed.

The experimental data displayed in Figure 9-11 also indicate that the emitting Ar species is principally formed by the e-beam rather than the sustainer discharge and that the resulting fluorescence is noticeably localized in regions at 3.55 - 3.65 and 3.95 - 4.05 microns. The

similar intensities displayed in Figure 9a and Figure 11b support the conclusion that the e-gun directly produces the Ar emission detected. Normalizing the peak intensities observed in Figure 9 and Figure 10 for the cases with no absorber cells by the integrated transmission of the "filter windows" produces the results tabulated in Table I and plotted in Figure 12. It should be noted that the argon peaks observed at 3.6 and 4.0 microns confirm earlier tentative reports of Ar emission at these wavelengths in bremsstrahlung experiments.[2] Of the two argon peaks, that at 3.6 microns would be expected to be absorbed by ground state HCl while that at 4.0 microns would not. This expectation is borne out by the observed attenuation of the Ar emission by HCl absorber cells, as is listed in Table I.

The Ar emission at 3.6 microns poses a serious obstacle to the detection of unambiguous HCl fluorescence data in the 3-4 micron region. Before turning to attempts to circumvent this problem, two final characteristics of the data obtained at 0.01% HCl should be mentioned. First, although the decay time and 22% absorption by an HCl absorber cell strongly indicate that Ar is the emitting species, Ar excitation is no longer explicable in terms of the e-beam as it was for the case of pure argon. The sustainer discharge plays an important role in exciting Ar after the e-beam terminates. This can clearly be seen in comparing Figure 8

where the sustainer is applied in conjunction with the e-gun and Figure 13 where only the e-gun is fired into a 0.01% HCl mixture. When only the e-gun is fired the results are identical to those obtained in pure argon shown in Figure 11. Also interesting is the noticeably greater sustainer current measured in the 0.01% HCl cases in Figure 8 compared to those for pure argon in Figure 9-10. This is despite the known rapid electron depleting action of dissociative attachment to HCl. The current traces obtained for the 0.01% HCl cases indicate that there is a sufficient electron density for the sustainer discharge to excite Ar when the e-gun terminates. This relatively slow decay of the electron density is in keeping with discharge predictions that, at this concentration of HCl, the discharge should be controlled by Ar_2^+ dissociative recombination rather than dominated by HCl dissociative attachment.

h. HCl Overtone Fluorescence

Because monitoring the HCl(v=1) population in 0.01% HCl mixtures through 3-4 micron emission proved unworkable, an attempt was made to use overtone emission in the two micron region to follow the temporal behavior of HCl(v=3). However, it was found that argon also emits in this region as can be deduced by applying the previous analysis of the 3-4 micron emission in 0.01% HCl mixtures to the 2-2.5 and 1.5-2.0 micron fluorescence from the same mixtures. These

data are shown in Figure 8c-8f. The same temporal behavior is displayed in both the 2-2.5 and 3-4 micron regions. The fluorescence in the 1.5-2.0 micron region was much weaker and displayed a less marked peak 0.8 μsec after e-gun crowbarred. The lack of significant attenuation of the fluorescence in the 1.5-2.5 micron region by the HCl/Ar absorber cell strongly indicates that in this case, where HCl self-absorption in the discharge region is of secondary importance and hence $v=2 \rightarrow v=0$ overtone emission should be an important contribution, the fluorescence is primarily due to argon. Hence all the oscillographs in Figure 8 are probably records of argon fluorescence.

i. Alternative Diluents

Helium was also used as a diluent in an attempt to avoid the 3-4 micron emission produced by argon. However, it was found that helium also emits in this region. Another diluent alternative investigated was hydrogen. Hydrogen did not emit in the 3-4 micron region, but it was not possible to sustain stable discharges in H_2/HCl mixtures at the voltages required for efficient HCl vibrational excitation.

j. HCl Pulsed Chemical Probe Laser

The most direct solution to these rare gas emission problems is to use an HCl pulsed chemical laser to probe the discharge region as a monitor of HCl vibrational populations. An apparatus recently used in HCl chemical laser

fuel experiments has been adapted to conduct these gain measurements by modifying the power supply so that longer duration (approximately 10 microseconds) laser pulses are obtained. After characterizing the output of this grating-tuned laser an extensive series of probe measurements will be undertaken.

2.2 Discharge Parameter Determinations

During this reporting period many other relative concentrations of HCl in one atmosphere of argon were briefly studied to determine the maximum voltage which could be sustained as a function of relative HCl concentration and e-gun foil distance. These results are presented in Figure 14 with the corresponding E/N_{HCl}. When these maximum voltages were exceeded, arcing would occur shortly after the e-gun was crowbarred. In the higher relative HCl concentration cases these discharge arcs tend to destroy the e-gun foil or the HCl absorber cell because of the high voltage involved. For these measurements at 0.1, 1, 5 and 10% HCl the sustainer current, sustainer voltage, e-gun voltage, and 3-4 micron emission were monitored. The electrical characteristics of the discharge will be compared with the predictions of the discharge code once a reliable set of cross-section data is assembled.

2.3 HCl Cross Section Studies

At present there is considerable controversy concerning the shape and overall magnitude of the HCl cross section for vibrational excitation. Because this cross section is of critical importance for an e-beam sustained discharge-excited HCl laser a brief review of recent measurements and calculations of this cross section is warranted. Using the transport data of Bailey and Duncanson[3] UARL employed the Frost and Phelps[4] analytical methods to calculate a complete set of HCl cross sections [5]. These calculations produced the HCl vibrational cross section shown in Figure 15. With a peak value of 1.5×10^{-15} cm^2 and a FWHM of about 0.5 eV this cross section was surprisingly large and strongly favored the feasibility of an electric discharge pumped HCl laser. Contemporaneous with the UARL analytical studies, were a series of experimental measurements of this cross section by Ziesel, Nenner and Schulz[6] in the region of 0 to 0.5 eV above threshold at 0.37 eV. In this experimental study the absolute magnitude of the HCl vibrational cross section was determined by comparing the trapped-electron current with the Cl^- current from HCl dissociative attachment, and correcting the trapped-electron current for the electron energy spread and for the contribution from elastically scattered electrons which are trapped. Consequently the absolute value of the HCl

vibrational cross section obtained is dependent on the HCl dissociative attachment cross section used. Ziesel, Nenner and Schulz used the value 1.95×10^{-17} cm^2 for the Cl^-/HCl cross section.[7] This produced a peak value of the HCl vibrational cross section of 1.2×10^{-15} cm^2, in excellent agreement with the UARL results. Moreover the experimental slope of the cross section from 0.37 eV to 0.52 eV, agreed very closely with the UARL calculation.

Rohr and Linder[8] recently reported a new experimental determination of the HCl vibrational cross section having roughly the same slope and peak as the UARL cross section but having only one third the width of the UARL cross section in the 0-1 eV region. However, this unfavorable narrowing was offset by the appearance of a broad secondary peak from 1.25 to 4 eV as is shown in Figure 15. Schulz[9] has also recently measured one point on this curve at approximately 2.8 eV which is in striking agreement with the Rohr and Linder[8] results. However, even more recently, Rohr and Linder[10] have concluded that their cross section is roughly 1.5 times as large as they originally thought, giving it a peak value of about 2.25×10^{-15} cm^2. This observation, if confirmed, would significantly increase the feasibility of the HCl electric discharge laser. Preliminary discharge calculations completed at PSI using the original Rohr and Linder cross section shown in Figure 15

indicate that although the low energy peak is narrower, by increasing the E/N_{HCl} from 0.8×10^{-15} V cm^2 to 1.0×10^{-15} V cm^2 a fractional electron power transfer to HCl vibrational excitation of 80% to 85% can still be maintained. As is indicated in Figure 14, this falls well within the accessible range of the NRL e-beam sustainer.

2.4 Proposed Experiments

Hence cautious optimism is justified that under the correct sustainer voltage significant HCl (v=1) excitation will be observed in the next reporting period. Once this is achieved an attempt will be made to produce and maximize gain on higher lying HCl vibrational transitions by monitoring such gain as a function of mixture composition and temperature using the HCl probe laser. Finally the effect of adding D_2 to such Ar/HCl mixtures will be determined. In all these efforts, theoretical modelling carried out in conjunction with PSI will serve as a means of interpreting data obtained and as a guide in the search for optimum operating conditions.

References

1. G. E. Caledonia (private communication), June 1975.
2. R. L. Taylor (private communication), May 1975.
3. V. A. Bailey and W. E. Duncanson, Phil. Mag., 10, 145 (1930).

4. L. S. Frost and A. V. Phelps, Phys. Rev., 127, 1621 (1962).

5. J. A. Shirley, B. R. Bronfin, W. L. Nighan, and T. L. Churchill, "E-Beam HCl Laser", UARL Report L911340-3, November 1972.

6. J. P. Ziesel, I. Nenner and G. J. Schulz, "Vibrational Excitation and Transmission Spectroscopy in Hydrogen Halides", 27th Annual Gaseous Electronics Conference, Houston, 1974.

7. L. G. Christophorou, R. N. Compton and H. W. Dickson, J. Chem. Phys., 48, 1949 (1968).

8. K. Rohr and F. Linder, "Low Energy Electron Scattering by Polar Molecules: Beam Experiments for the e-HCl System", IX International Conference on the Physics of Electronic and Atomic Collisions, Seattle, 1975.

9. G. J. Schulz (private communication), July 1975.

10. K. Rohr and F. Linder (private communication), July 1975.

Table I - Attenuation of Ar Emission by Various Filters and Absorber Cell

FILTER BANDWIDTH[a] (microns)	PEAK SIGNAL NO ABSORBER CELL (μV)	FILTER WINDOW[b]	PEAK SIGNAL FILTER WINDOW	SIGNAL/WINDOW NORMALIZED	PEAK SIGNAL WITH ABSORBER CELL[c] (μV)	%ABSORPTION
3.1698-4.3131	247	116.6	2.12	1	202	18.2
3.9176-4.4269	188	42.7	4.40	2.08	178	5.3
3.7078-4.0736	260	44.8	5.80	2.74	232	10.8
3.4416-3.6890	107	35.3	3.03	1.43	82	23.4
3.5857-3.6656	80	10.3	7.77	3.66	50	37.5
3.9683-4.0816	110	10.1	10.89	5.14	110	0

a Bandwidth limits determined by wavelengths at which transmission drops to 50% of maximum transmission.

b Filter window is integrated area of transmission vs wavenumber curve.

c 40-cm long absorber cell was filled with 300 torr HCl/300 torr Ar.

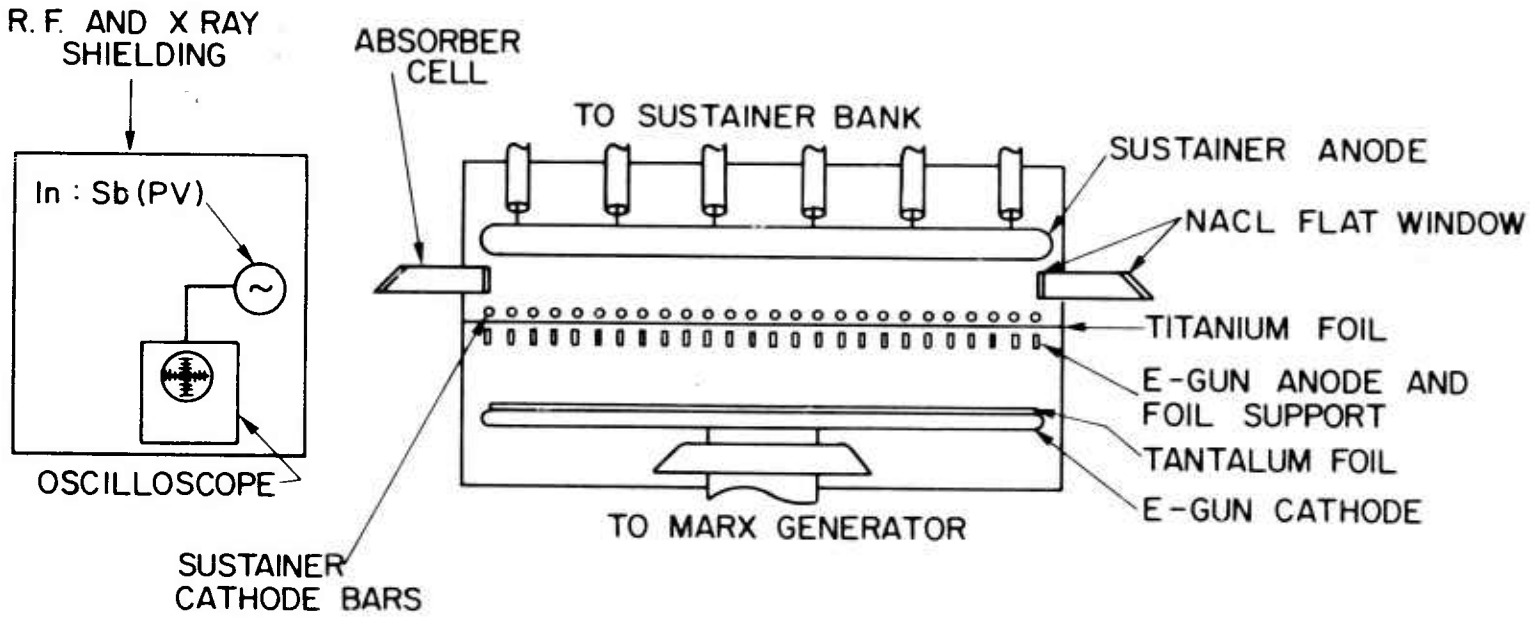

Fig. 6 - HCl fluorescence measurements

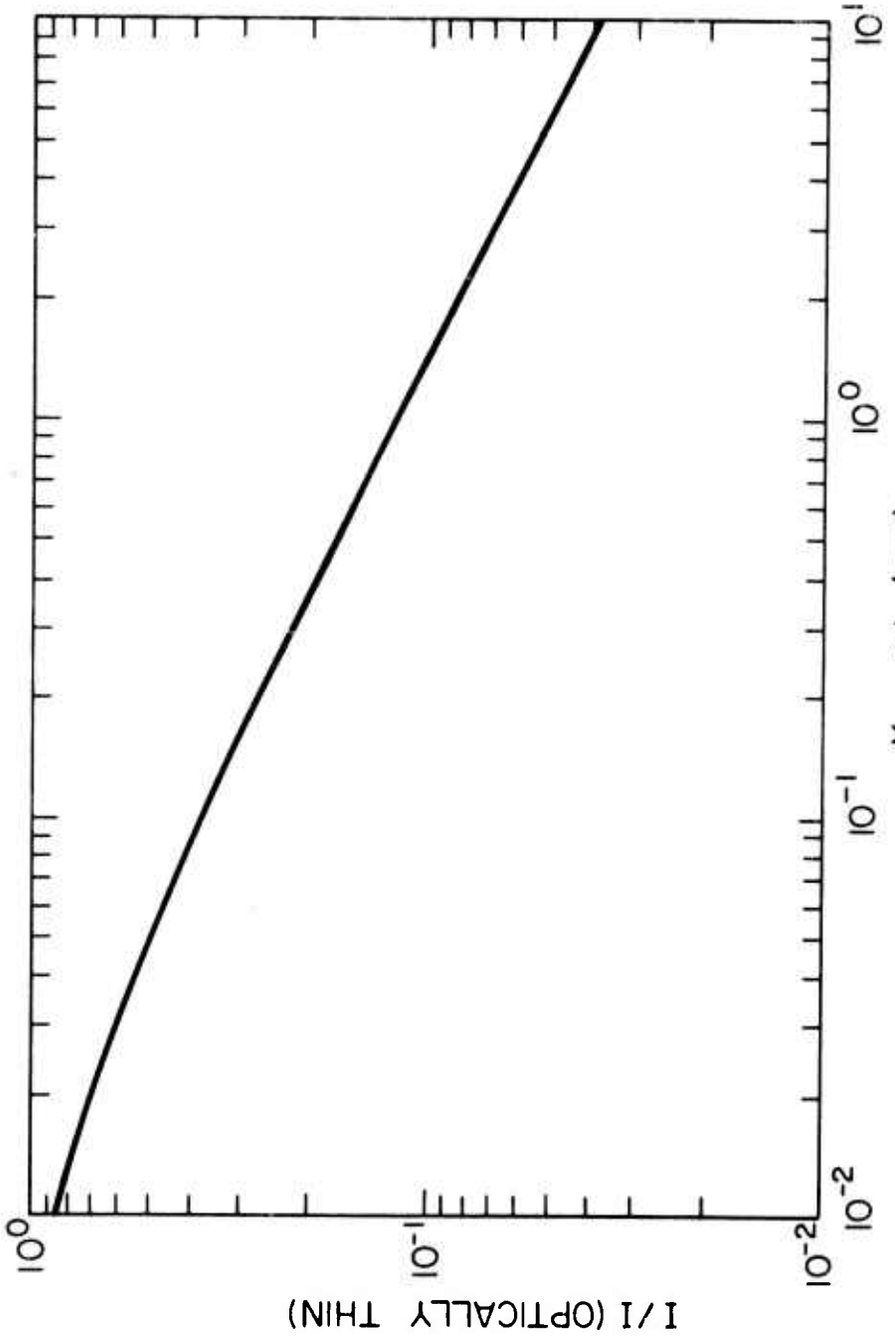

Fig. 7 - Effect of self-trapping on relative intensity for HCl^{35} fundamental band, P_1-P_4, Lorentz broadened Ar/HCl mixtures, P_{total} = 760 Torr

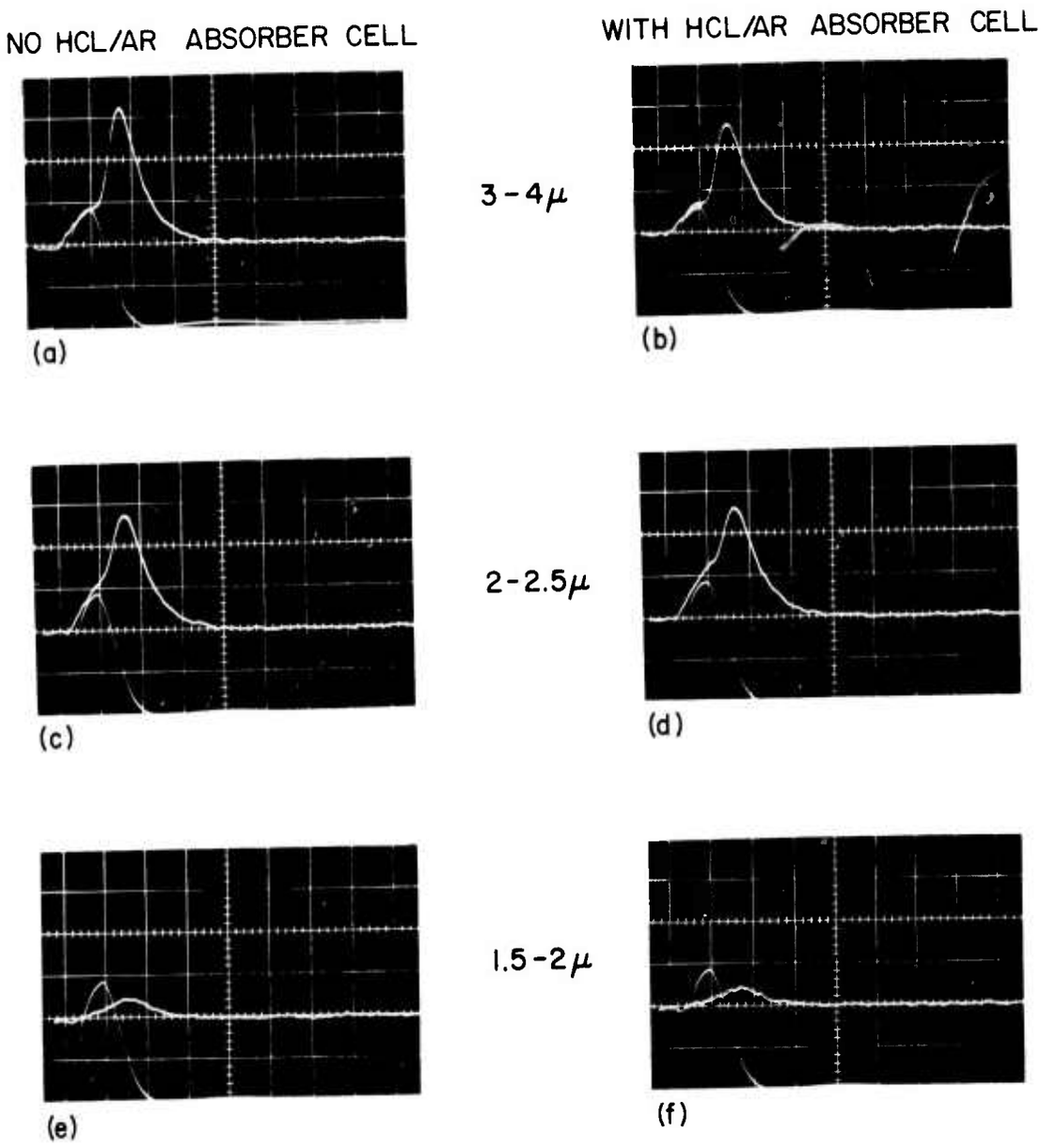

Fig. 8 - Fluorescence and sustainer current for 0.01% HCl/Ar 760 Torr mixture excited by e-beam sustainer discharge

† = 2 μsec/div I_s = 0.75 A-cm^{-2}/div

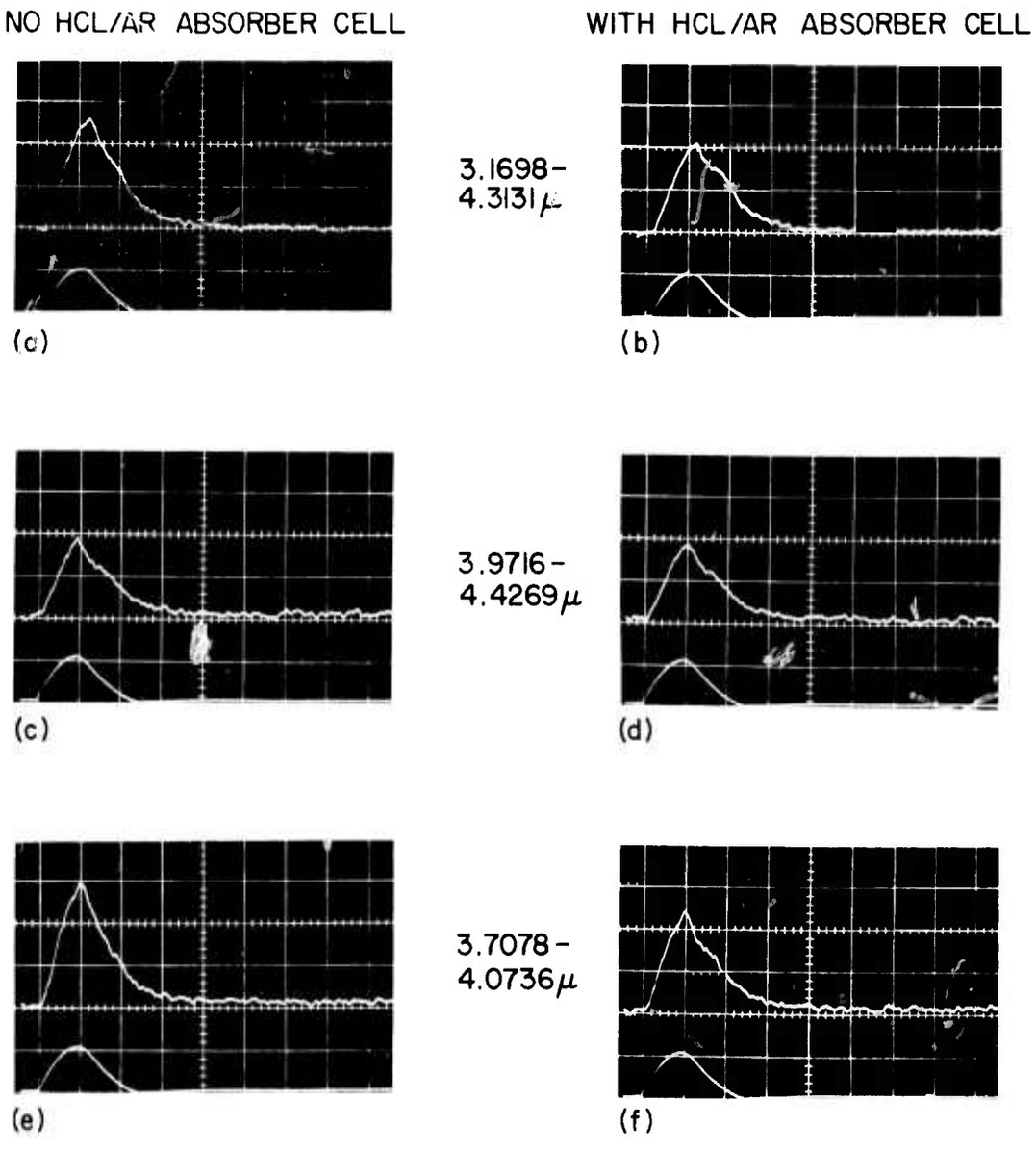

Fig. 9 - Fluorescence and sustainer current for 760 Torr Argon excited by e-beam sustainer discharger

† = 2 μsec/div I_s = 1.5 A-cm^{-2}/div

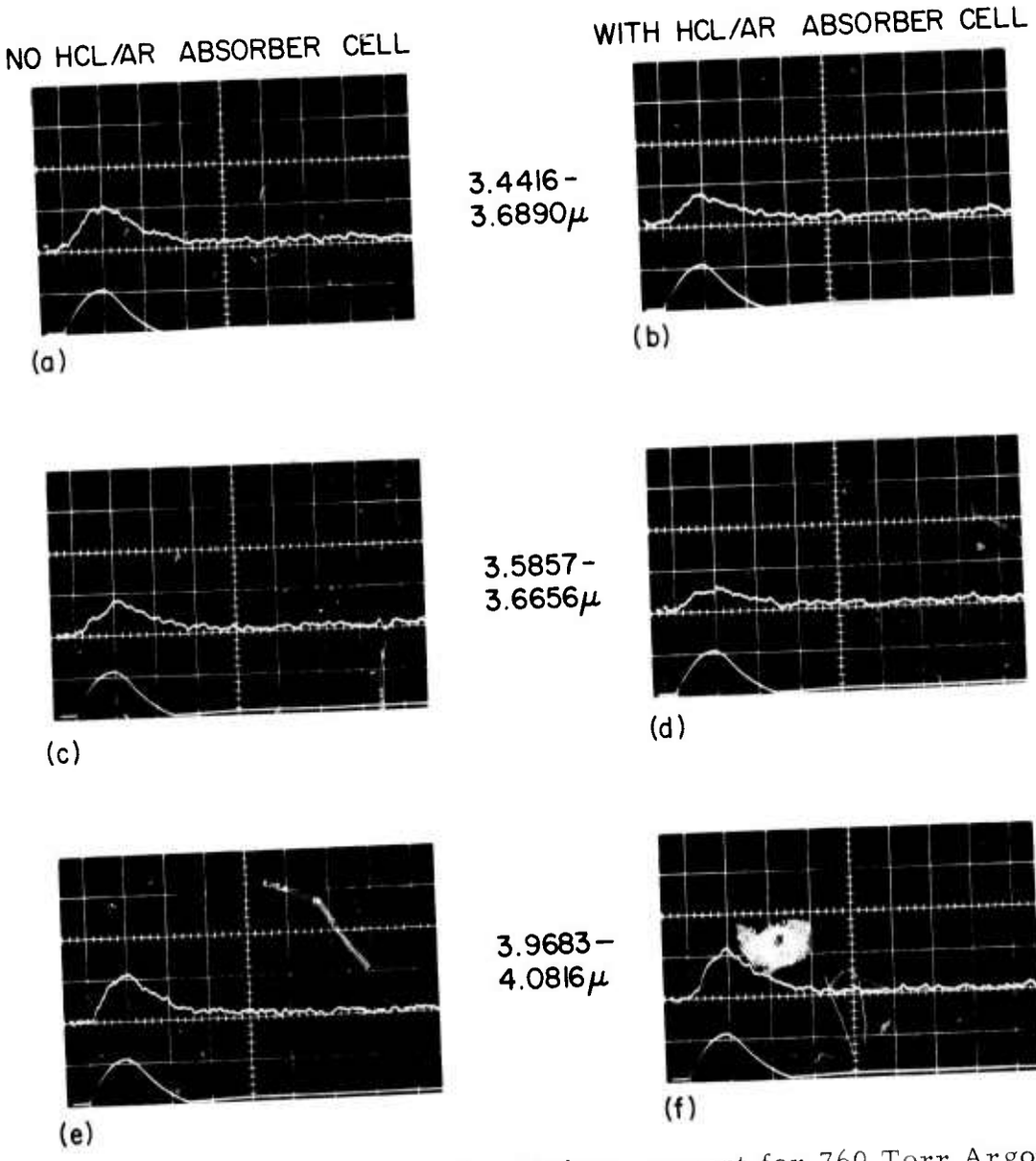

Fig. 10 - Fluorescence and sustainer current for 760 Torr Argon excited by e-beam sustainer discharge

† = 2 μsec/div I_s = 1.5A-cm^{-2}/div

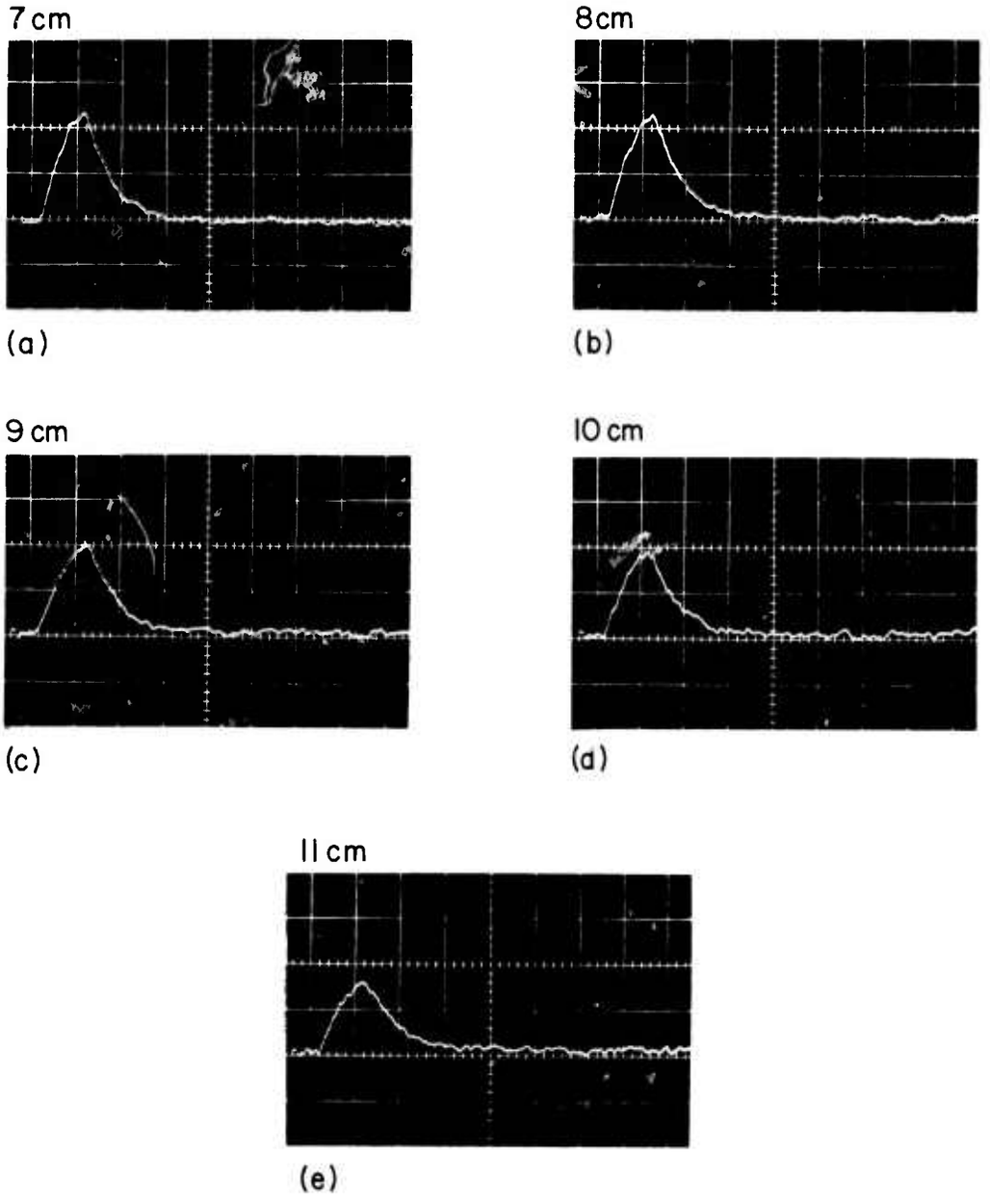

Fig. 11 - 3-4 μ fluorescence from 760 Torr Argon excited i 2 μsec e-beam pulse for various cathode-foil distances

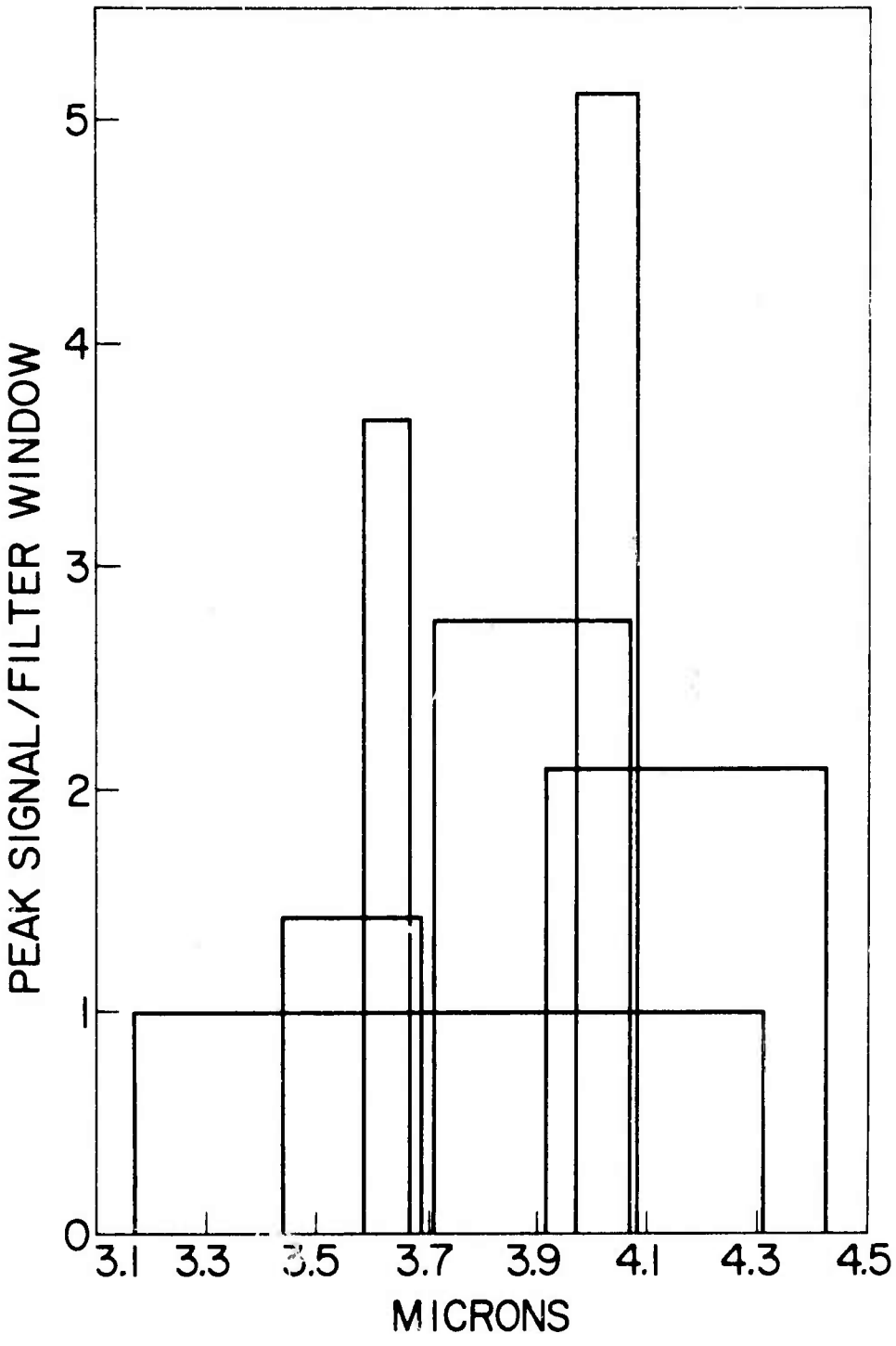

Fig. 12 - Fluorescence from e-beam sustainer excited Argon as transmitted by filters

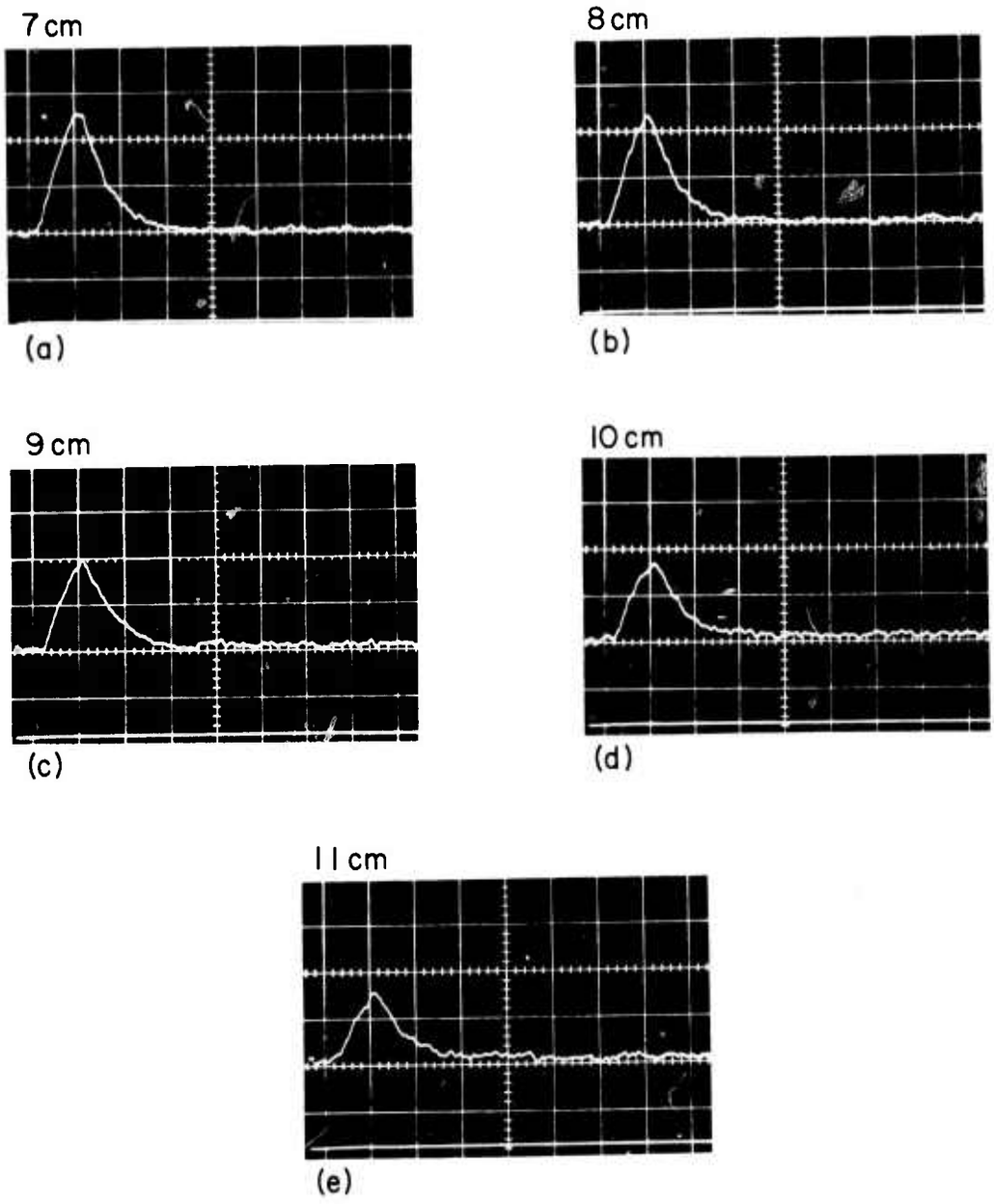

Fig. 13 - 3-4 μ fluorescence from 0.01% HCl/Ar 760 Torr mixture excited by 2 μsec e-beam pulse for various cathode-foil distances

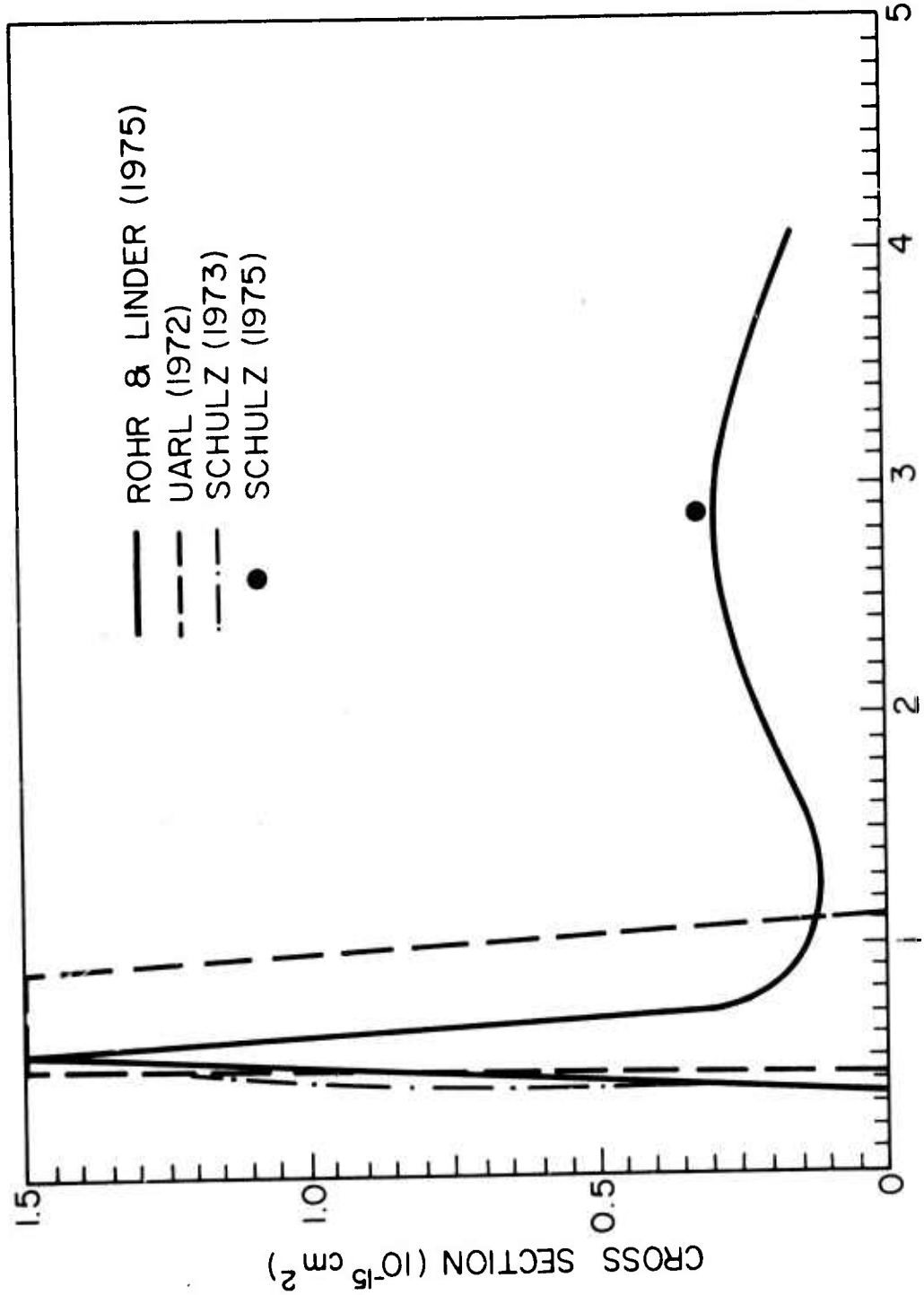

Fig. 14 - HCl vibrational excitation cross section

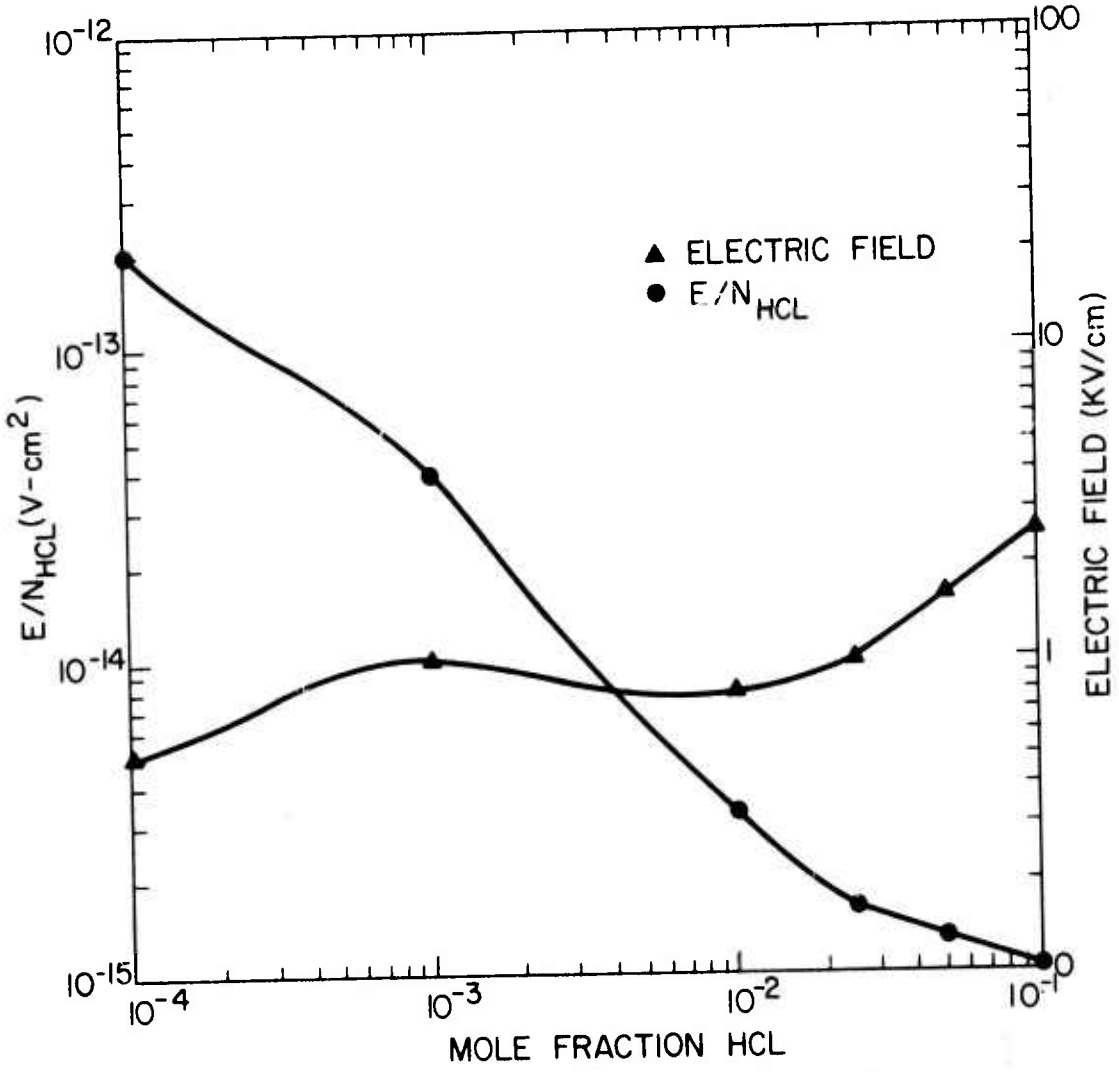

Fig. 15 - Maximum sustainer electric field vs mole fraction HCl for 760 Torr Ar/HCl mixtures

ELECTRONIC STATE LASERS

1. Electron Beam Initiated Visible Transition Lasers

In previous work the NRL e-beam facility was used to discover, develop, and characterize the Ar-N_2 energy transfer laser. Techniques were created for making quantitative fluorescence measurements, for calculating excited state production, and for computing the temporal concentrations of the transient species. During the course of the Ar-N_2 research these techniques were applied to the Xe-Br_2 system during the current reporting period with considerable success. We report here the discovery of the first rare gas-halide laser and its associated kinetics.

Our interest in the rare gas-halide lasers stemmed from a recent note by Setser and Velazco.[1] They reported emission from the rare gas-monohalides for the first time and suggested these species as laser candidates. We selected Xe-Br_2 from the list of laser candidates because its strong fluorescence in the afterglow experiments, its fast reaction rate, its bound-free spectrum and the absence of absorption at the laser wavelength.[2]

Stimulated emission was observed from XeBr at 281.8 nm and the results of these experiments have already been

described in the literature.[3] Subsequently further work has been performed on the XeBr system and on the yields of excited state species.

Appendices B and C provide details of the experiments and the relevant conclusions. In the future we plan to fully characterize the XeBr laser emission and then to pursue experiments with the heated laser cell.

References

1. J. E. Velazco and D. W. Setser, J. Chem. Phys., 62, 1990 (1975).

2. A. A. Passchier, J. D. Christian, and N. W. Gregory, J. Chem. Phys., 71, 938 (1967).

3. S. K. Searles and G. A. Hart, Appl. Phys. Letters 27, 243 (1975).

2. Pulsed Metal Vapor Laser

During this reporting period data has been collected on the transverse discharge system, detailed in the last report, operated as a copper vapor laser from CuCl. A schematic of the tube is shown in Figure 16.

The initial results of the device are charted in Table I. Each column corresponds to a separate set of conditions.

After analyzing this data, a number of changes were made in the system to improve the laser output. The initial system had a central inlet for buffer gas, with a

TABLE I

Peak Power	2 kw	1.2 kw
Pulse Width	10 ns	20 ns
Pulse Energy	18 μJ	24 μJ
Active Volume	$\leq$ 50 cm^3	$\leq$ 50 cm^3
Buffer gas - Argon	30 torr	5 torr
Output Coupling	8%	80%
Energy in Storage Capacitor	.6 Joules	.6 Joules

reservoir for CuCl located in this gas line, just outside of the main tube. This reservoir was eliminated and the CuCl distributed along the bottom of the tube in an effort to obtain a higher CuCl vapor density and a more homogeneous distribution. The Brewster angle mounts were modified to restrict the diffusion of CuCl vapor to the windows. In order to increase the amount of energy available to dissociate the CuCl (or Cu_3Cl_3) molecules on the first pulse, the storage capacitor for that pulse was increased from .008 μf to .1 μf.

The .1 μf capacitor is labeled Cs_1, on Figure 17, which details the discharge circuitry of the device. The two pulses necessary for the laser are produced by the two thyratron circuits. When a thyratron fires, its associated storage capacitor begins to charge the set of capacitors C_D, which are closely coupled to the laser electrodes. At gas

breakdown, these latter capacitors dump their energy into the discharge, through a low inductance connection. The risetime and pulse width of the discharge pulse depends upon the impedence of the circuit consisting of the "dumping" capacitors and the laser tube only. When the system is operated as a copper laser, the very fast risetime and short pulse width detailed in the last report are not necessary for highest power output. Raising the C_D capacitance to 9.3 nf doubled the energy available to the discharge, while the risetime increased to only 15 ns and the pulse width to < 50 ns. These experimental conditions were used to obtain the data reported here.

Vacuum distillation of the cupious chloride to remove impurities and water vapor was found to be unnecessary. Loading the tube with CuCl and heating to 150°C to outgas the CuCl worked as well or better than the separate distillation. As a result more CuCl could be loaded and refill time was also much reduced.

Helium, neon and argon were compared as buffer gases with neon giving the best results. Lasing was observed at temperatures from 300°C to 500°C and at pressures of 75 to 100 torr. A plot of peak power vs. pressure for a temperature of 385°C and 130 μs delay between pulses is shown in Figure 18. Figure 19 shows the variation in peak power with time delay. The temperature dependence seems to follow that

observed by Russell et al.[1] The best results are listed in Table II.

Table II

Peak Power	11 kW
Pulse Width	10 ns FWHM
Energy/Pulse	~ 100 μJ
Specific Energy	12 $\mu J/cm^3$
Temperature	390°C
Ne Pressure	20-30 Torr
Pulse Delay	130 μs
Peak Current	6000 A

The pressure dependence observed has been the subject of some concern. The question is whether the inverse dependence of power on pressure is real or due to some systematic defect in the device. Recently, Piper[2] has observed a much different dependence of peak power vs. neon pressure for a CuI transverse discharge laser of somewhat different design. He has observed a peak in power vs. pressure at 150 torr, with electrode separation of 2.5 cm and capacitor voltage of 20 kV. The maximum output power from a 70 cm long tube at 150 torr was about the same as that observed in the NRL device at 20-30 torr.

Evidence that some systematic defect may be responsible is that, at higher pressures of neon, ~ 200 torr, the

discharge very noticeably tracks along the quartz liner. Since it is hard to observe the discharge at lasing pressures, it is possible that this tracking phenomenon occurs even at low pressures, only becoming noticeable at ~ 200 torr. Furthermore, earlier results using argon at 30 torr were found to be no longer reproducible after the neon data were taken, indicating some new systematic effect was occurring which limited the operating pressure range of the device. This effect could have been tracking along the walls, as the result of the formation of a CuO film due to a leak in the tube. Further work has begun to resolve this question. Should the source of the pressure falloff be remedied, and the output power of the device to scale with pressure as in Piper's device,[2] an order of magnitude improvement in specific energy and output power would occur.

The specific energy observed to date is estimated to be 12 $\mu J/cm^3$ if one assumes an active region only 2 mm wide. This is to be compared with the 20 $\mu J/cm^3$ reported by Russell[1] for a double-discharge CuCl device. However, it is anticipated that substantial improvement in output and efficiency will occur when the transverse discharge is scaled up, eliminating dileterious discharge - wall interactions. Solution of this problem will allow the true potential of the transverse discharge design to be evaluated.

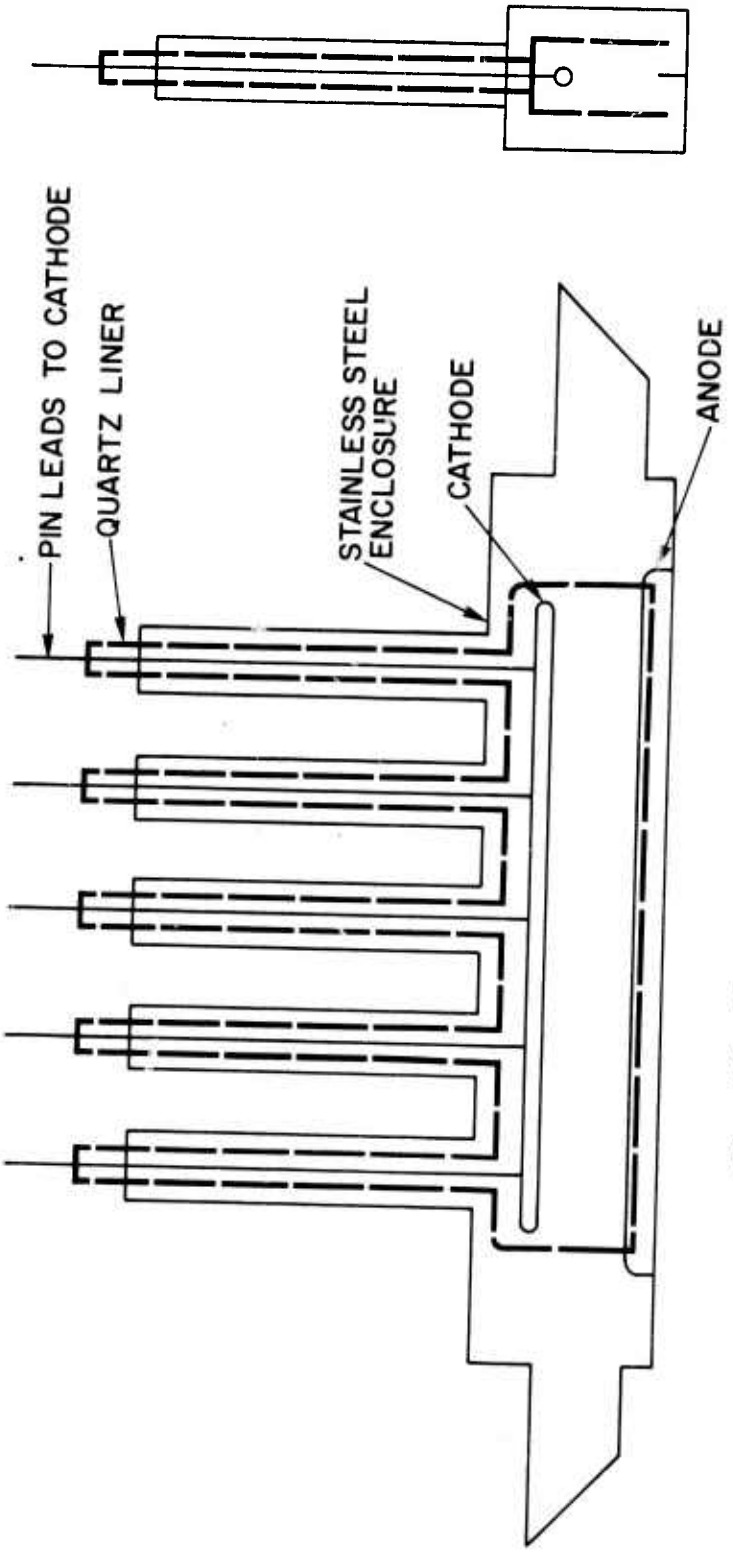

Fig. 16 - Transverse discharge laser apparatus

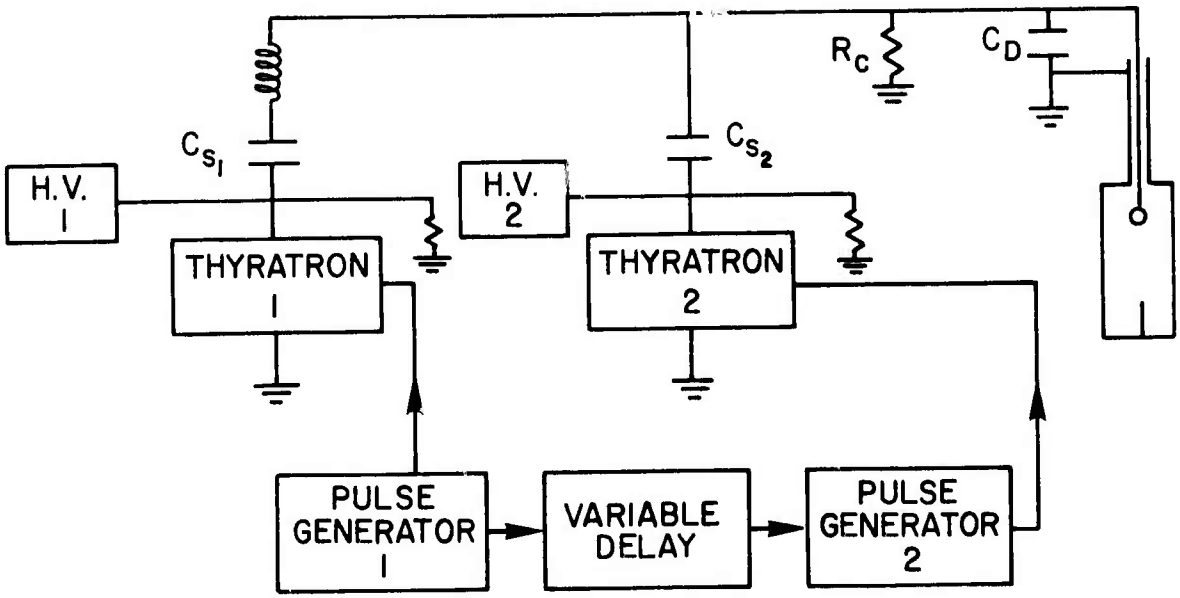

Fig. 17 - Transverse discharge circuit diagram

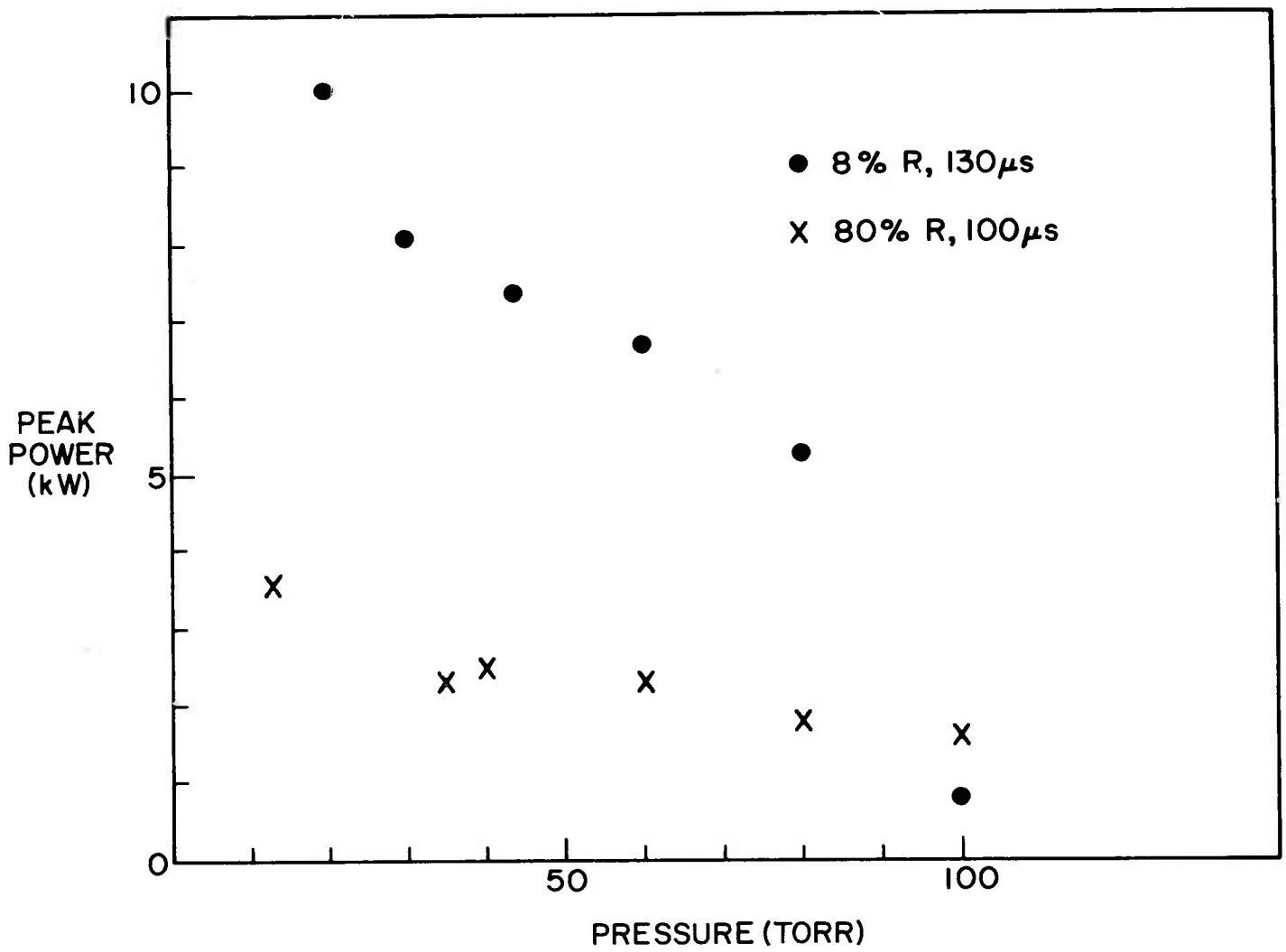

Fig. 18 - Variation of Cu laser peak power vs pressure.
T = 385°C, delay between pulses 130 μsec.

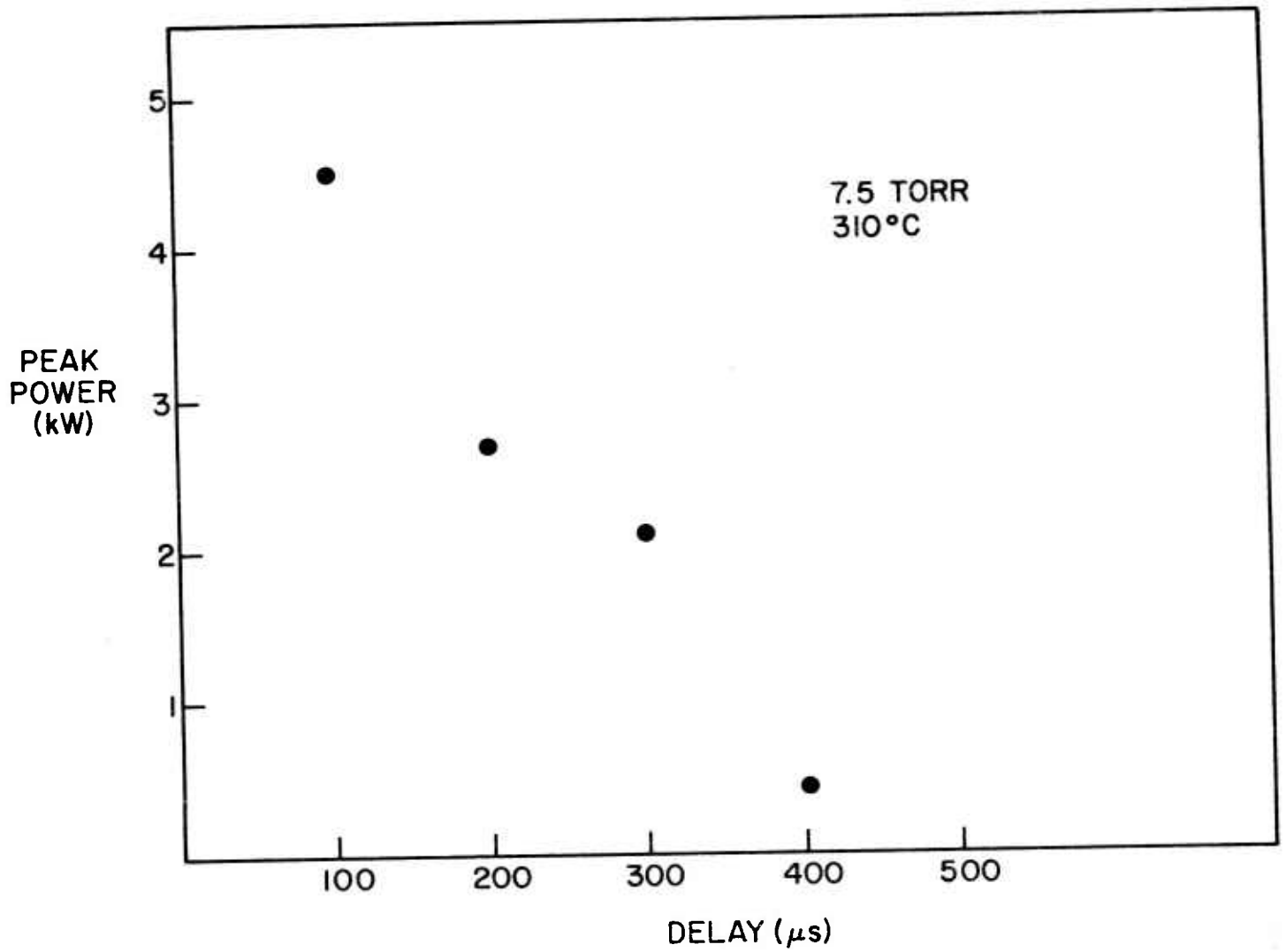

Fig. 19 - Variation of Cu laser peak power with time delay
T = 360°C P = 7.5 Torr

References

1. Visible Wavelength Laser Development, Third Quarterly Report to DARPA by J.P.L., G. R. Russell, Program Manager.

2. J. A. Piper, "A Copper Iodide Laser Excited by Transverse Discharge", Opt. Comm. 14, 296, 1975.

3. Mercury-Sodium Energy Transfer Experiments

The process of electronic state energy transfer between the $6p\,^3P$ states of mercury and near resonant s, p, d, and f states of sodium has been proposed as an efficient mechanism for the production of population inversions in sodium. The specific steps in the production of the inversion are given below:

$$Hg(^1S_0) + E(5eV) \rightarrow Hg(^3P_{1,0}) \qquad 1a$$

$$Hg(^3P_{1,0}) + Na(3s\ ^2S) \rightarrow Hg(^1S_0) + Na^* \qquad 1b$$

$$Na^* \rightarrow Na^{**} + h\nu \qquad 1c$$

The energy of excitation of the mercury ^3P states, E, may be supplied either through electrical or optical pumping. Na* and Na** represent upper and lower excited states of sodium connected by an optical transition with a photon energy $h\nu$.

Two approaches to the excitation scheme given above have been investigated. The results of the investigations indicate that the production of population inversions of the magnitude required for efficient operation of visible

lasers in sodium is unlikely to be achieved by the proposed mechanism. Study of the mercury-sodium transfer system has therefore been suspended. A brief description of our experiments with this system is given below.

The first study concerned the possibility of obtaining laser action on the Na(7f - 3d) transition at 9961Å. The Na(7f) state is resonant with the Hg($^3P_1$) state which was excited in a conventional electrical discharge in a mixture of mercury and sodium vapors with argon as a carrier gas. A quartz hollow-cathode discharge tube was built which was equipped with brewster-angle windows and separate reservoirs for mercury and sodium metal. The device was contained within an oven and the temperatures of the reservoirs of mercury and sodium were controlled independently and monitored with thermocouples. Argon flowed over the quartz brewster-windows in order to protect them from corrosion by sodium vapor. The discharge tube had a diameter of 0.8 cm and the discharge current through the tube could be varied between 0.1 and 1.0 Amperes. The gas mixture was typically 10-50 torr argon, 0.1-1.0 torr Hg and 0.01-0.1 torr Na. The density of atoms in the Na(7f) state was determined from measurements of the spontaneous emission from the discharge on the 9961Å transition which were made using a calibrated photo-diode and a narrow band filter of known transmission. The sensitivity of the detector was such that populations of

the Na(7f) level corresponding to optical gains of less than 1% along the 50 cm active length of the discharge tube could have been detected.

No emission at 9961Å was detected for any combination of operating conditions which was tried. Even with large ratios of the Hg to Na concentrations, most of the electrical excitation went into the Na(3p) resonance levels. The presence of mercury therefore had little effect on the distribution of excited states of sodium in the discharge.

A second set of experiments were conducted in which specific optical excitation of the Hg($^3P_1$) state was substituted for the electrical excitation. For the purpose of these experiments a concentric electrodeless discharge lamp-optical pumping cell was constructed. The lamp was made of quartz in order to transmit the 2537Å optical pumping radiation, and was powered by a 1000W magnetic induction discharge. The optical pumping cell was constructed with an active region approximately 6 inches long which was made of 1/4 inch o.d. single-crystal sapphire tubing. All other parts of the cell were made of stainless steel to resist corrosion by sodium vapor. Brewster end windows were protected from corrosion by flowing argon. The entire lamp and optical pumping cell was designed to be raised to 500°C. The sodium vapor pressure in the discharge cell was temperature controlled in a side oven. The pressure of the mercury

vapor in the cell was maintained at approximately 2 microns in order to assure proper absorption of the 2537Å pumping radiation across the 4 mm I.D. of the optical cell.

Initial experiments were conducted in which the steady state population of the $Hg(^3P_1)$ state was determined from absorption measurements at 4358Å along the length of the active region. These experiments yielded a value of $10^{11}/cm^3$ for the density of $Hg(^3P_1)$ atoms. The density of sodium vapor was next increased by raising the temperature of the Na reservoir. At an estimated sodium density of about $10^{15}/cm^3$ observation of the fluorescence from the optically pumped cell revealed the presence of emission from excited states of Na. The most intense sodium lines were those at 5686Å and 6159Å. These lines are assigned to the Na(5s-3p) and Na(4d-3p) transitions whose upper states are not resonant with the $Hg(^3P_1)$ level. Population of the 5s and 4d levels of sodium is felt to be due to radiative and collision-induced cascading from higher lying levels. Since the 5686Å and 6159Å lines were most intense, estimates of their upper state densities were made through comparison of the intensities of these lines to emission on the 5461Å mercury line. The estimated populations of the Na 5s and 4d levels were of the order of $10^7/cm^3$. Attempts to increase the populations of these states beyond this were unsuccessful. Since these populations were a factor of 50 from those

estimated to be required for successful laser action it was decided that work on the Hg-Na transfer system should be discontinued.

4. Visible Laser Diagnostics - Lifetime Measurements in HgBr

The measurement of the radiative lifetime of the $B(^2\Sigma^+)$ state of HgBr was completed during this reporting period as part of a study to evaluate the HgBr(B→X) transitions as a potential laser system.[1] The choice of that particular system as a laser candidate was made on the basis of the known large Franck-Condon displacement between the $B(^2\Sigma^+)$ and $X(^2\Sigma^+)$ states.

The method adopted for the measurement was optical excitation with a short laser pulse accompanied by the monitoring of the decay of the perturbed $B(^2\Sigma^+)$ state molecules through their spontaneous emission. The initial states for the optical pumping are levels near V=20 in the $X(^2\Sigma^+)$ state of HgBr created by a discharge pulse in $HgBr_2$. A nitrogen-laser-pumped dye laser with pulse width of less than 10 nsec was used to excite these HgBr molecules into the lowest vibrational levels in the $B(^2\Sigma^+)$ state. The laser induced fluorescence signal was viewed at 90° to the pump laser beam with a fast-rise photomultiplier tube. This signal was observed to have a simple exponential decay with a half-life of 18±3 nsec. This decay time was independent of the wavelength of the excitation laser pulse indicating that the

radiative lifetime does not vary with upper state V. The absence of any pressure dependence of the decay time confirmed it as the true radiative lifetime.

The laser pulse was applied after the discharge pulse at the end of a variable delay. The amplitude of the laser induced fluorescence signal decreased with increasing delay reflecting a loss of species in the levels pumped by the dye laser. At long times after the discharge pulse, the amplitude of the signal was observed to decrease by about a factor of two in 1 μsec. This decay rate is interpreted as the rate of loss of species near V=20 in the $X(^2\Sigma^+)$ state by vibrational relaxation or reactive collisions.

Following these lifetime measurements, a 1/2-meter transverse discharge apparatus was built for laser action investigations. The device had a current risetime faster than 20 nsec. Experiments with a laser cavity around the cell did not result in lasing. Gain measurements were then performed using the Ar laser at 496.5 nm and 501.7 nm, which correspond to regions of intense emission in HgBr. Only absorption was observed over the range of temperature and diluent pressure conditions which could be tested.

The technique of laser induced fluorescence in a pulsed discharge has proven to be useful for studying transitions which terminate in transient states and/or species. When properly applied, one can obtain information on the lifetime of both the upper and lower states involved.

5. Visible Chemical Laser Experiments

a. Flash Photolysis Study of the $O(^1S_o)$ + CO and $O(^1D_2)$ + CO Reactions

Recently it has been demonstrated that rare gas atoms (Xe, Kr and Ar) induce the forbidden $O(^1S_o) \rightarrow O(^1D_2)$ transition leading to the generation of stimulated emission at 557 nm. Since CO relaxes the $O(^1S_o)$ atom at a rate 10 times faster than that of Ar, the possibility of laser action from the reaction $O(^1S_o)$ + CO has been examined. N_2O was employed as the $O(^1S_o)$ atom source

$$N_2O + h\nu\ (\sim 120\ nm) \rightarrow O(^1S_o) + N_2$$

since the quantum yield of this reaction is known to be unity at ~ 120 nm. The proposed chemical pumping is based on the reaction sequence:

$$O(^1S_o) + CO(X\ ^1\Sigma^+) \rightarrow CO_2^{**}\ (^1\Sigma_g^+)$$

$$CO_2^{**} \rightarrow CO_2^*\ (^1A_2 \text{ or } ^1B_2) + h\nu\ (557\ nm)$$

$$CO_2^*\ (^3A_2 \text{ or } ^3B_2) \rightarrow O(^3P) + CO(X^1\Sigma^+, v).$$

To date, after several attempts with varying experimental conditions, laser oscillation at 557 nm has not yet been achieved. Detailed spectroscopic studies of this system and other reactions such as N + CX (X = F, H and CO) are planned to be carried out with a newly acquired sensitive Optical Multichannel Analyzer (OMA) system.

Intimately related to the $O(^1S_o)$ - CO system is the dynamics of the $O(^1D_2)$ + CO reaction. If instead of the

reaction scheme proposed, the CO acts to induce the $O(^1S_o) \rightarrow O(^1D_2)$ transition, then the $O(^1D_2)$ + CO reaction serves to remove the population of the lower laser level. It is known that the $O(^1D_2)$ atom is deactivated by CO within about 10 collisions. The question arises as to how the 45.4 kcal/mole of the electronic energy carried by the $O(^1D_2)$ atom is released during the collision. As shown in Figure 20, the $O(^1D_2)$ state is in close resonance with the vibrational levels of CO at v=7 and 8. One would expect a complete CO vibrational population inversion if the relaxation reaction took place via such resonance transfer processes.

A cw CO laser probing system has been set up to investigate the dynamics of this fundamentally important E → V energy transfer process:

$$O(^1D_2) + CO\ (X\ ^1\Sigma^+,\ v=0) \rightarrow O(^3P) + CO\ (X\ ^1\Sigma^+,\ v=?)$$
$$\Delta E = 45.4 \text{ kcal/mole}$$

Experimentally, mixtures of O_3 and CO were photolyzed in a co-axial quartz flash tube and the population of CO at various levels were determined by time-resolved resonance CO laser absorption. O_3 was employed as the $O(^1D_2)$ atom source based on the photolytic reaction, $O_3 + h\nu\ (\geq 200\ nm) \rightarrow O(^1D_2) + O_2$. From these experiments, the CO formed in the $O(^1D_2)$ + CO reaction was found to be vibrationally excited up to v=7, which is the limit of available electronic energy

carried by the excited O atom. The vibrational temperature of CO, as shown in Figure 21, was determined to be about 8000 ± 100°K indicating no total population inversion. The efficiency of the E → V energy transfer at 293°K was found to be 21 ± 1%.

The present results indicate quite clearly that the $O(^1D_2)$ + CO reaction does not take place via a resonant, impulsive type collision, but rather, via a complex-forming mechanism. The latter mechanism is strongly supported by the results of quantum statistical calculation according to the Rice-Ramsperger-Kassel-Marcus (RRKM) theory and its semiclassical RRK version (see Figure 21). The fact that these statistical theories predict quantitatively the observed CO vibrational population distribution indicates that the electronic energy carried by the $O(^1D_2)$ atom is indeed completely randomized within all degrees of freedom during the complex-forming collision:

$$O(^1D_2) + CO \rightarrow {}^1CO_2^* \rightarrow {}^3CO_2^* \rightarrow O(^3P) + CO(v \leq 7)$$

where ${}^1CO_2^*$ and ${}^3CO_2^*$ represent electronically excited singlet ($^1A_2$ or $^1B_2$) and triplet ($^3A_2$ or $^3B_2$) CO_2 molecules, respectively.

The above mechanism is further evidenced by the result of an isotope-labeled experiment using $C^{18}O$. The data shown in Figure 22 were obtained from the flash photolysis of the 1:1:8 mixtures of O_3-CO-SF_6 and O_3-$C^{18}O$-SF_6, both carried

out under exactly the same experimental conditions. These data show that the $O(^1D_2)$ + $C^{18}O$ reaction yields $C^{16}O$ (v) at a rate about half that of the total rate of CO (v) production. This observation can only be accounted for by the complex-forming mechanism mentioned above, and thus rules out unequivocally the so-called half collision, or impulsive collision model for this reaction.

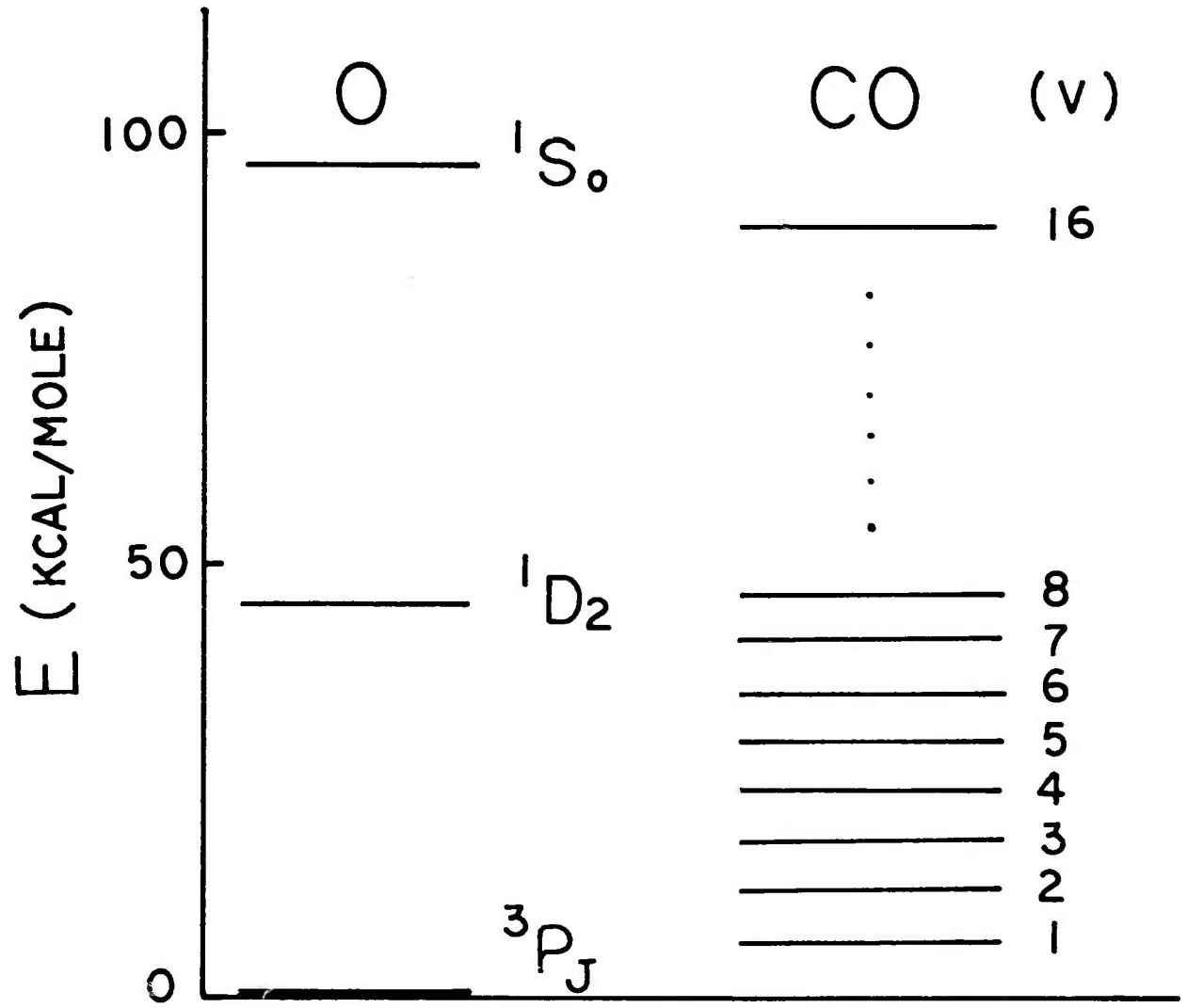

Fig. 20 - Energy levels of 0 atom and CO(v=n)

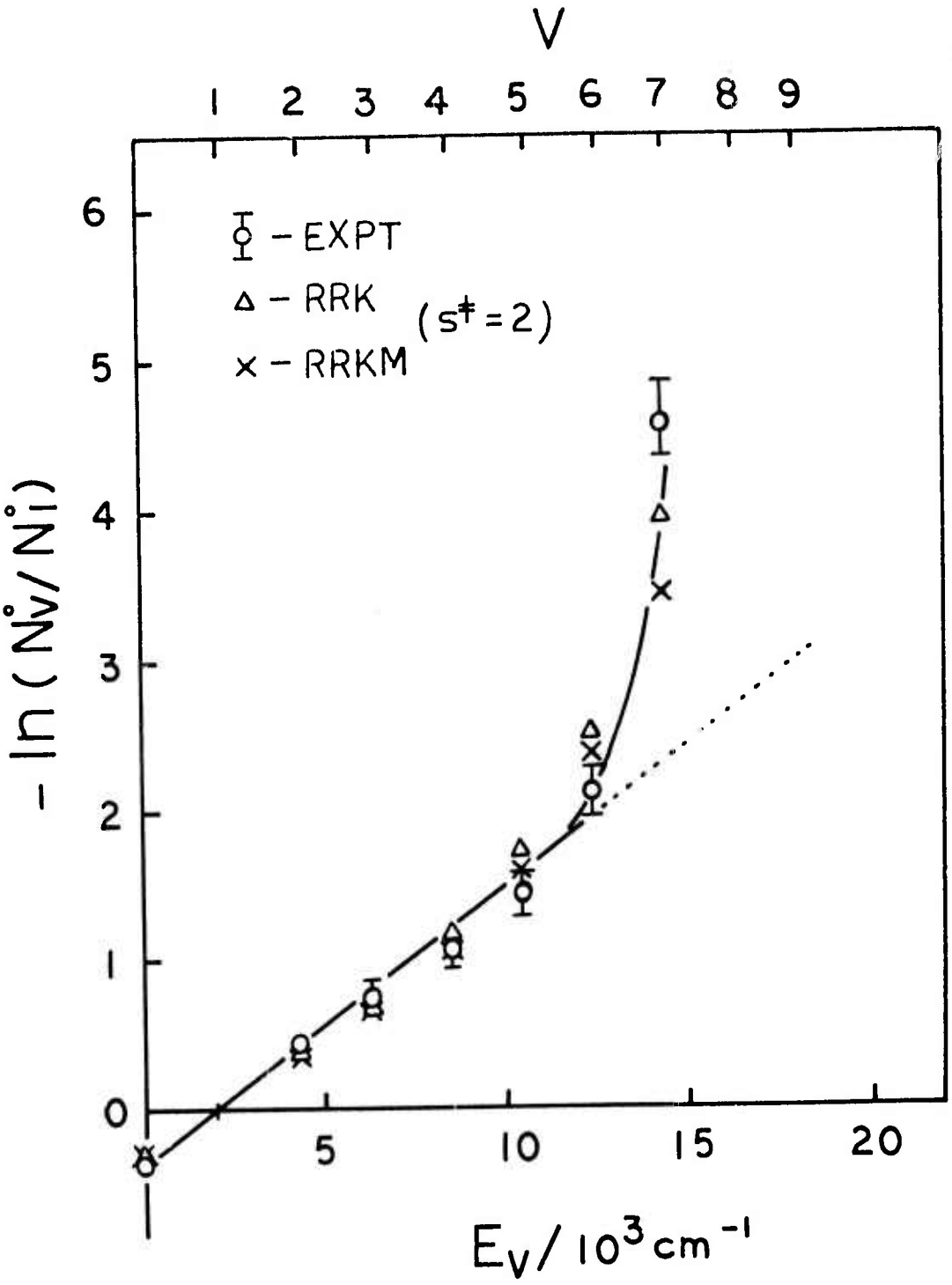

Fig. 21 - Boltzmann Plot of CO(v=n) population distribution

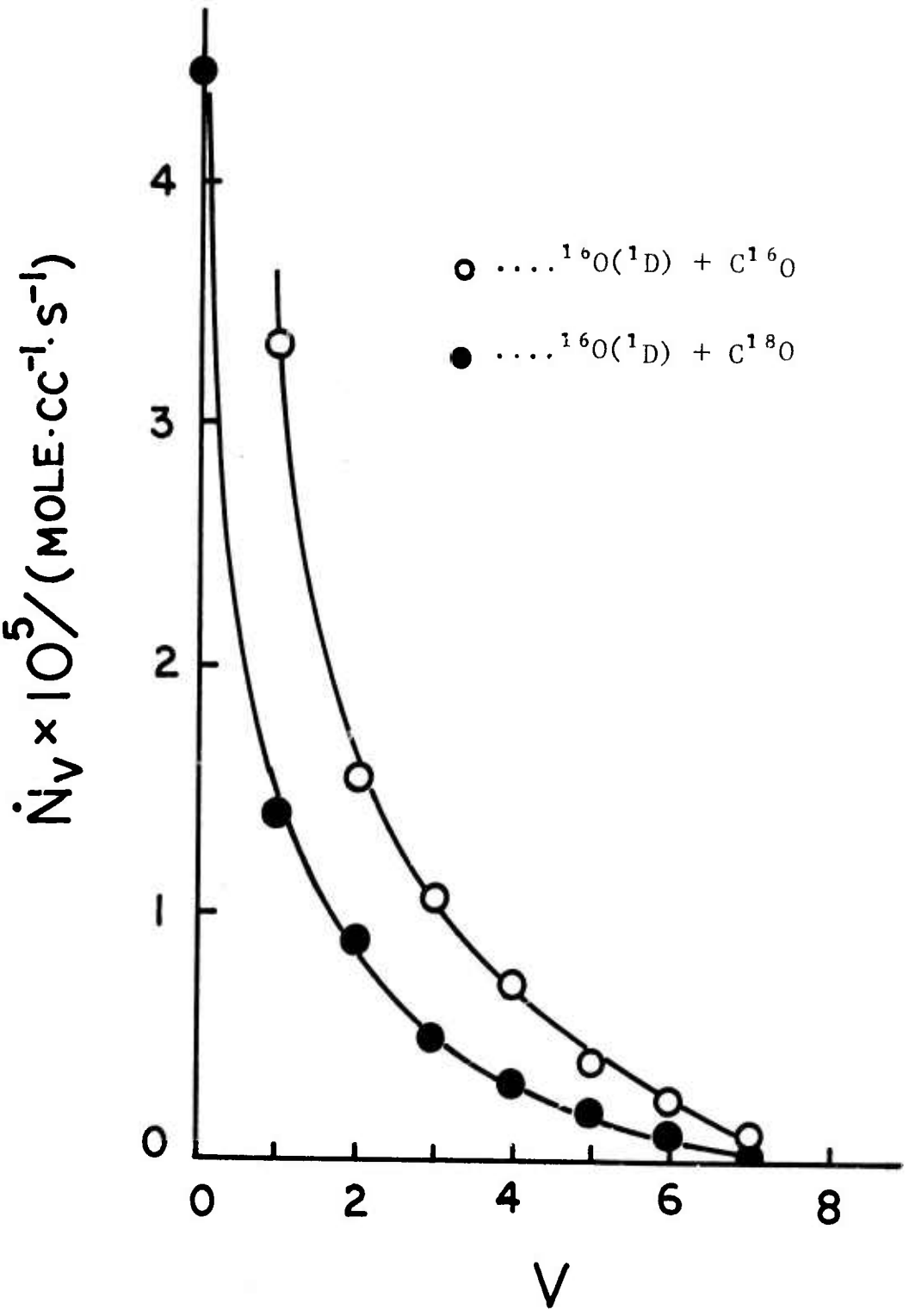

Fig. 22 - Rate of production of $C^{16}O_{(v=n)}$

APPENDIX A

FUELS FOR A PREMIXED PULSED HCl LASER

T. J. Manuccia, J. A. Stregack, and W. S. Watt

Abstract

HCl pulsed chemical lasing was obtained from several premixed R-Cl/HI mixtures when initiated by a transverse pulsed discharge. The relative merits of these mixtures were compared to a premixed H_2/Cl_2 mixture. For a constant stored electrical energy several mixtures have been found which give higher specific power than the H_2/Cl_2 system. In addition, it has been possible to run some of these improved mixtures without diluent with no laser performance degradation.

The first pulsed chemical HCl laser was reported by Kasper and Pimentel[1] in 1965. Since then, several workers[2-7] have studied various fuel systems which produced HCl lasers using both flashlamp and pulsed discharge initiation of the chemical reactions. However, no attempt to quantify the relative merits of these fuel systems has been undertaken. Consequently, an investigation of many of the fuel systems previously studied as well as several new fuels was undertaken to compare their relative merits in producing HCl laser radiation.

Typically, pulsed HCl lasers operate using either the H_2/Cl_2 mixture which has the assumed reaction sequence

$$Cl + H_2 \rightarrow HCl + H \qquad - 1 \text{ kcal/mole} \qquad (1)$$

$$H + Cl_2 \rightarrow HCl^* + Cl \qquad + 45 \text{ kcal/mole} \qquad (2)$$

or the HI/Cl_2 system which operates on the two exothermic reactions

$$H + Cl_2 \rightarrow HCl^* + Cl \qquad + 45 \text{ kcal/mole} \qquad (3)$$

$$Cl + HI \rightarrow HCl^* + I \qquad + 32 \text{ kcal/mole} \qquad (4)$$

In the H_2/Cl_2 system, endothermic reaction (1) is slow on the time scale of the laser pulse and therefore contributes neither to the production of excited HCl nor to the supply of H atoms for reaction (2). The requisite H atoms must come directly from the dissociation of H_2 in the discharge. HI is a better source of atomic hydrogen than H_2 and one would expect the HI/Cl_2 system to be more efficient.

However, premixing of HI and Cl_2 is difficult to perform without spontaneous reaction. Alternate chlorine sources, R-Cl, were sought which would be sufficiently reactive so that the resulting HI/R-Cl mixture would outperform the H_2/Cl_2 system and, in addition, could be premixed with HI.

The laser used in the present study is a transverse electrical pin discharge laser which is constructed from aluminum tubing. The discharge region was 100 cm long with 100 evenly spaced ballasted (1 kΩ, 1 W) cathodes (Stupkopf connectors electrically isolated from the outer tube) located approximately 2.5 cm from a hemicylindrical brass anode. The electrical initiation of the chemical reactions was provided by repetitive discharge (typically 1 pps) of a 0.0027-μF capacitor charged to a voltage of 30 kV. The optical cavity was formed by two gold mirrors, one of which had an on-axis 0.5 mm hole through which the output power was coupled. The pairs of gases were premixed before entering the laser region and a small amount of He was injected as window purge. Laser radiation was detected with a Ge:Au detector. As the pulse shapes were very similar when each of the fuel-oxidizer mixtures was optimized, performance was determined from peak pulse heights.

Initial experiments performed on the apparatus gave the result that the H_2/Cl_2 mixture produced laser power which was about one order of magnitude greater than the

HI/Cl_2 mixture. There was clear evidence of prereaction in the HI/Cl_2 system which could explain its lower power. An additional factor is that vibrational excitation of the H_2 or production of Cl* in the discharge for the H_2/Cl_2 experiment could make reaction (1) exothermic and promote chain behavior, with a subsequent increase in H_2/Cl_2 laser output. Efficient electron impact excitation of H_2 has been observed.[8]

In order to compare the merits of the various fuels, an initial screening was performed by adding the proposed chlorine atom source to an HCl laser operating on the H_2/Cl_2 system. These runs were made with the laser operating chlorine lean such that the effect of the new chlorine source would be as large as possible. Those fuels which either enhanced or did not degrade lasing were CCl_4, CCl_3H, PCl_3, $COCl_2$, $TiCl_4$, $SOCl_2$, $SnCl_4$, CCl_3CH_3, CCl_2CHCl, CCl_2F_2, CF_3CCl_3, and C_6H_5Cl. As a result of this screening, several of these systems and one other have led to HCl lasing in premixed R-Cl/HI systems. New Cl atom sources not previously reported in the literature which produced HCl laser emission are $SiCl_4$, $SnCl_4$, CF_3CCl_3, CCl_3CH_3, CCl_2CHCl, C_6H_5Cl, PCl_3, and $TiCl_4$. In addition, lasing was observed using CCl_4,[7] CCl_3H,[7] $SOCl_2$,[6] and CCl_2F_2[7] as had been previously reported.

By optimizing conditions for each pair of fuels (at constant stored electrical energy), it has been possible to identify those fuel sources that operate at higher specific powers (power out per mole of reactants) than the H_2/Cl_2 system. These improved laser fuels and their optimized operating characteristics are summarized in Table I. The H_2/Cl_2 mixture preferred to operate in the range $0.5 < H_2:Cl_2 < 15$ with optimum operation occurring at a fuel to oxidizer ratio of 2. The HI/R-Cl mixtures all optimized at fuel-to-oxidizer ratios below 0.5 and lasing could never be maintained beyond a ratio of 2.0. The previously reported experiments[7] on the HI/CCl_4 and HI/CCl_2F_2 systems were performed under conditions of high helium dilution (> 90 percent). In the present experiments these fuel mixtures were run with less than 3 torr of He, which plays little or no part in the kinetics. For example, laser power was not affected when all helium was removed from the CCl_2F_2/HI system. One anomalous effect was observed when the output more than doubled when the 3 torr of He were removed from the $TiCl_4/HI$ system.

As reported by Taylor,[7] HF and HCl lasing occurred simultaneously for the CCl_2F_2/HI mixture. In the present experiments, for the optimum HCl lasing conditions the HCl laser output was approximately 2.5 times that of HF.

References

1. J. V. V. Kasper and G. C. Pimentel, "HCl Chemical Laser," Phys. Rev. Lett., Vol. 14, pp. 352-354, 1965.

2. J. R. Airey, "A New Pulsed I-R Chemical Laser," IEEE J. Quantum Electron. (Notes and Lines), Vol. QE-3, p. 208, May 1967.

3. T. F. Deutsch, "New Infrared Laser Transitions in HCl, HBr, DCl, and DBr," IEEE J. Quantum Electron. (Notes and Lines), Vol. QE-3, pp. 419-421, Oct. 1967.

4. C. B. Moore, "An Electrically Pulsed HCl Laser," IEEE J. Quantum Electron., Vol. QE-4, p. 52, Feb. 1968.

5. M. C. Lin, "HCl Chemical Laser from H + Cl_2O," Chem. Phys. Lett., Vol. 7, pp. 209-210, Oct. 15, 1970.

6. J. R. English, III, H. C. Gardner, R. W. Mitchell, and J. A. Merritt, "HCl Chemical Lasers with $SOCl_2$, SO_2Cl_2, Cl_2CNCl, and ClCN," Chem. Phys. Lett., Vol. 16, pp. 180-182, Sept. 15, 1972.

7. D. Taylor, S. W. Mayer, and S. N. Suchard, "HCl Chemical Lasing with HI and Chloro Compounds," IEEE J. Quantum Electron. (Corresp.), Vol. QE-10, pp. 389-390, Mar. 1974.

8. J. A. Stregack and B. L. Wexler, "A New Electric Discharge Gasdynamic Laser," presented at the 4th Conf. Chemical and Molecular Lasers, St. Louis, Mo., Oct. 21-23, 1974.

References

1. J. V. V. Kasper and G. C. Pimentel, "HCl Chemical Laser," Phys. Rev. Lett., Vol. 14, pp. 352-354, 1965.

2. J. R. Airey, "A New Pulsed I-R Chemical Laser," IEEE J. Quantum Electron. (Notes and Lines), Vol. QE-3, p. 208, May 1967.

3. T. F. Deutsch, "New Infrared Laser Transitions in HCl, HBr, DCl, and DBr," IEEE J. Quantum Electron. (Notes and Lines), Vol. QE-3, pp. 419-421, Oct. 1967.

4. C. B. Moore, "An Electrically Pulsed HCl Laser," IEEE J. Quantum Electron., Vol. QE-4, p. 52, Feb. 1968.

5. M. C. Lin, "HCl Chemical Laser from H + Cl_2O," Chem. Phys. Lett., Vol. 7, pp. 209-210, Oct. 15, 1970.

6. J. R. English, III, H. C. Gardner, R. W. Mitchell, and J. A. Merritt, "HCl Chemical Lasers with $SOCl_2$, SO_2Cl_2, Cl_2CNCl, and ClCN," Chem. Phys. Lett., Vol. 16, pp. 180-182, Sept. 15, 1972.

7. D. Taylor, S. W. Mayer, and S. N. Suchard, "HCl Chemical Lasing with HI and Chloro Compounds," IEEE J. Quantum Electron. (Corresp.), Vol. QE-10, pp. 389-390, Mar. 1974.

8. J. A. Stregack and B. L. Wexler, "A New Electric Discharge Gasdynamic Laser," presented at the 4th Conf. Chemical and Molecular Lasers, St. Louis, Mo., Oct. 21-23, 1974.

TABLE I

	PARTIAL PRESSURES OF OPTIMUM CONDITION (TORR)	LASER OUTPUT (NORMALIZED TO H_2/Cl_2)	SPECIFIC OUTPUT (OUTPUT/MOLE-NORMALIZED TO H_2/Cl_2)
$H_2/Cl_2/He$	(40/20/3)	1.0	1.0
$HI/CCl_2F_2/He$	(1/10/3)	4.0	18.0
$HI/CCl_4/He$	(1/7/3)	4.5	25.8
$HI/CF_3CCl_3/He$	(0.6/7.0/3)	3.1	18.4
$HI/TiCl_4/He$	(3.4/10/3)	1.0	3.8
$HI/TiCl_4$	(3.5/10)	3.0	14.0
$HI/PCl_3/He$	(2.0/4.2/3)	.4	2.7

APPENDIX B

YIELDS OF $N_2(C)$ FROM $Ar^* + N_2$ AND $XeBr^*$ FROM $Xe^* + Br_2$ †

S. K. Searles and G. A. Hart*

Abstract

Investigation of reactions I and II was

I $\quad Ar^* + N_2 \rightarrow N_2(C) + Ar$

II $\quad Xe^* + Br_2 \rightarrow XeBr^* + Br$

carried out by e-beam excitation of Ar-N_2 and Xe-Br_2 mixtures. Analysis of the fluorescence data and e-beam energy deposition led to yields of 0.20 $N_2(C)$ for Ar^* and 0.30 $XeBr^*$ for Xe^*.

† Work supported in part by DARPA.

* NRC-NRL Postdoctoral Research Associate (1973 - present).

INTRODUCTION

Short pulse high energy e-beams (electron beams) can be used to achieve laser emission by pumping high pressure gases. An understanding of the excited state reaction mechanism is necessary to allow comparisons to other laser candidate systems and to facilitate laser scaling predictions. We have previously proposed mechanisms for the Ar-N_2 and Xe-Br_2 systems.[1,2] The mechanisms were found to agree with time resolved fluorescence data. The essential part of each mechanism is given in Table I. In this paper we wish to report the branching ratios k_4/k_5 and k_{11}/k_{12} which directly limit laser efficiency. In a previous paper[1] we indicated a value for k_4/k_5 on the basis of elementary energy deposition calculations. In this paper we utilize a sophisticated transport code to evaluate the deposited energy and revise the ratio k_4/k_5. Details on the quantitative photometry are provided and a value for k_{11}/k_{12} is presented for the first time.

EXPERIMENTAL

The high energy e-beam facility has been described in earlier communications.[1,3] The diode assembly, laser cell, and photodiode which viewed side emission are illustrated in Figure 1. The e-beam device generated 50 ns long pulses of 433 kV electrons from a carbon cathode 15 cm x 1 cm. The electrons entered the laser cell through a foil support

consisting of 14 - 0.95 cm diameter holes lying on a straight line 15 cm long. Twenty-five micron thick Ti foil was used for the Ar-N_2 experiments while 37.5 microns thick Inconel 750-X foil was used for the Xe-Br_2 experiments since Ti reacts with Br_2. The 433 keV electrons encountered a cell of internal dimensions 1.27 cm x 1.27 cm x 15 cm in length perpendicular to the beam.

A knowledge of the beam uniformity is necessary to allow energy deposition calculations per unit volume. The integrated incident intensity was monitored by blue cellophane thin film dosimetry.[4] A read-out of the exposed film with a He-Ne laser indicated a background film transmission of 17.5% with bleached circular areas of 42.3 ± 2.3% transmission corresponding to the holes in the support plate.

The electrons passed through the thin gas targets and backscattered from the stainless steel cell walls causing a highly uniform deposition. Photographs of the side fluorescence from a 1 atm Ar-N_2 mixture verified the uniformity.[5]

Side fluorescence was received by an ITT F4018 high current S-5 photodiode through a sapphire window as illustrated in Figure 1. The ITT calibration curve for the specific photodiode was used to quantify the fluorescence intensities. A Tektronix 7904 scope with 50 ohm termination

recorded the detected signals. The sampled volume was a cylinder 0.95 diameter and 1.27 cm in length.

The intensity per unit excited volume was determined with the following additional information. The solid angle for light collection was 0.0225 steradians as defined by a distance of 12.5 cm from the center of the sampled volume to the photocathode surface of area 3.548 cm^2. The sapphire window introduced a transmission loss of 14%. A fine mesh screen with 50% transmission covered the face of the photodiode to reduce electrical noise. In addition Corning filters No. 5840 (330 - 380 nm) and No. 9863 (255 - 390 nm) were used to check for extraneous emission.

The energy deposition per unit volume was calculated from a knowledge of the e-beam energy per pulse of 36 J, the fraction of the energy absorbed by the gas as computed by the Transport Electron Program (TEP)[5,6], and the excited volume of 1.27 x 1.27 x 15 cm^3.

Figure 2 presents the TEP depth-dose plot for 433 keV electrons in Ar. The fractional energy loss was found to be 1.3%/cm atm for Ar and 5.2% atm for Xe at low pressure where the absorption is small. The deposited energy is related to the ion production by the W values of 26.2 for Ar and 21.9 eV/ion pair for Xe.[7] Peterson and Allen[8] have reported generation of 0.33 Ar* for each Ar^+. An extrapolation of their results to the case of xenon leads to a ratio of 0.33 Xe* for each Xe^+ created initially.

ARGON-NITROGEN SYSTEM

In the argon-nitrogen system preliminary results including representative oscillograms were previously reported for the Ar-N_2 system.[1] Here we present additional details and a revision of the branching ratio k_4/k_5 to reflect improvement in the energy deposition calculation. The original calculation neglected scattering because gas scattering is not significant at the densities under consideration. However, backscattering from the rear cell wall is significant. The TEP code includes this effect as well as a number of more subtle effects.[5,6] Figure 2 displays the deposition results for 433 keV electrons in Ar. The correction factor over the calculation without scattering is approximately a factor of three.

The deposition calculation was used to determine the excited state production terms as a function of time with the use of a trapezoidal shape to simulate the electron beam pulse shape as shown in Figure 1 of Reference 1. This dependence along with the rate equations arising from steps (1-8) listed in Table I was used to generate N_2(C-B) fluorescence curves through numerical integration by a Runge-Kutta-Treanor kinetics code.[9]

A comparison of the experimental N_2(C-B) fluorescence with the computer generated curves is given in Figures 3-4. The general agreement demonstrates the acceptability of the

mechanism. In the FWHM computations there were no adjustable parameters while in the $N_2(C)$ concentration plot, the magnitude was adjustable through k_4. The best fit gave k_4 the value of 6×10^{12}. Thus for each Ar* which is created by the e-beam and which reacts with N_2, 20% yields $N_2(C)$. The new value reported here is to be compared with the limit $\leq$ 17% established by Setser et al[10] for the reaction of argon metastables with N_2. The value can also be compared with 30% obtained by a different interpretation of e-beam induced fluorescence.[11]

XENON-BROMINE SYSTEM

The approach to the Xe-Br_2 system was different from the approach to the Ar-N_2 system. The Ar-N_2 system could be reliably analyzed over a wide pressure range because the numerous rate processes were well understood. In Xe-Br_2 the basic steps were reported only very recently. There is insufficient data to interpret the fluorescence at higher pressures. As a consequence the ratio k_{11}/k_{12} was evaluated at low pressures where the mechanism can be simplified to the one given in Table 1. The ionic processes are sufficiently slow that they do not contribute to the production of XeBr* on a time scale comparable to the direct steps 9 and 10.[2] Quenching of XeBr* is also relatively unimportant at low pressures. Thus plots of the integrated fluorescence signal with an extrapolation to zero pressure can

be used to ascertain the ratio k_{11}/k_{12}. Figure 5 shows two plots of the fluorescence versus percentage Br_2 for three total pressures. The extrapolation to zero bromine concentration eliminates the major XeBr* quencher. The integrated intensities are directly proportional to the total pressure since the e-beam deposition is directly proportional to the pressure. The zero bromine pressure intercepts when normalized by the total pressure are 3.43 (13.4 torr), 3.89 (27 torr) and 4.13 (54 torr) volt-nsec. The small scatter in these values may be due to a minor amount of quenching by Xe. Extrapolation of these values to zero pressure of xenon yields an intercept of 3.34 volts/torr. Conversion of the units by means of the TEP code and the detection calibration data leads to a value of 0.30 XeBr* per Xe* created by the beam. This value is 50% greater than that obtained for the Ar-N_2 system. This suggests that the Xe-Br_2 system holds greater promise for efficient laser emission. It is hoped that with further quantitative measurements some general conclusions can be made about the yields of electronically excited products from R*-additive collisions.

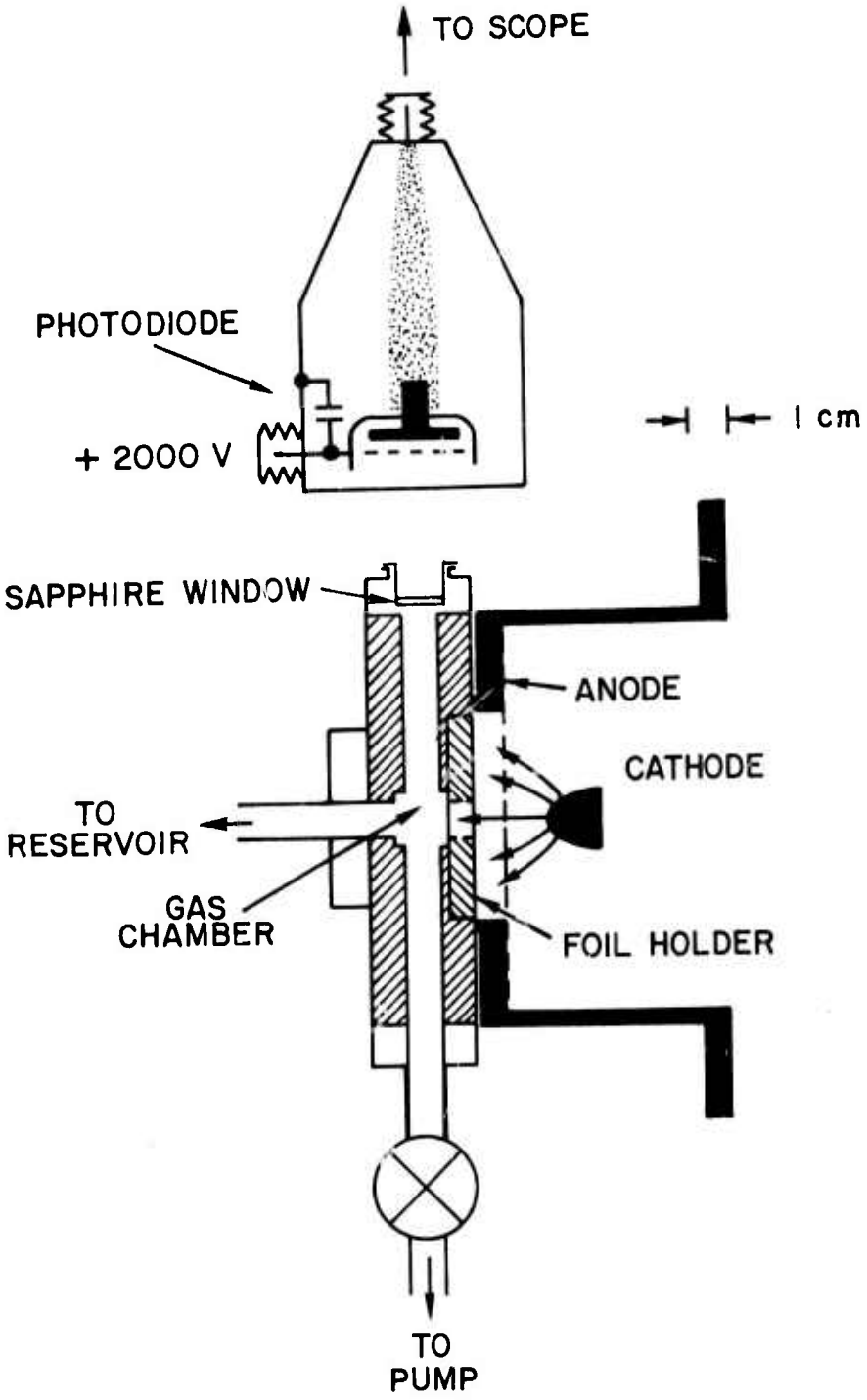

Fig. 1 - Experimental apparatus drawn to scale. A 433-keV electron beam entered the gas chamber and excited the rare gas-additive mixtures. Fluorescence was viewed in a direction perpendicular to the beam.

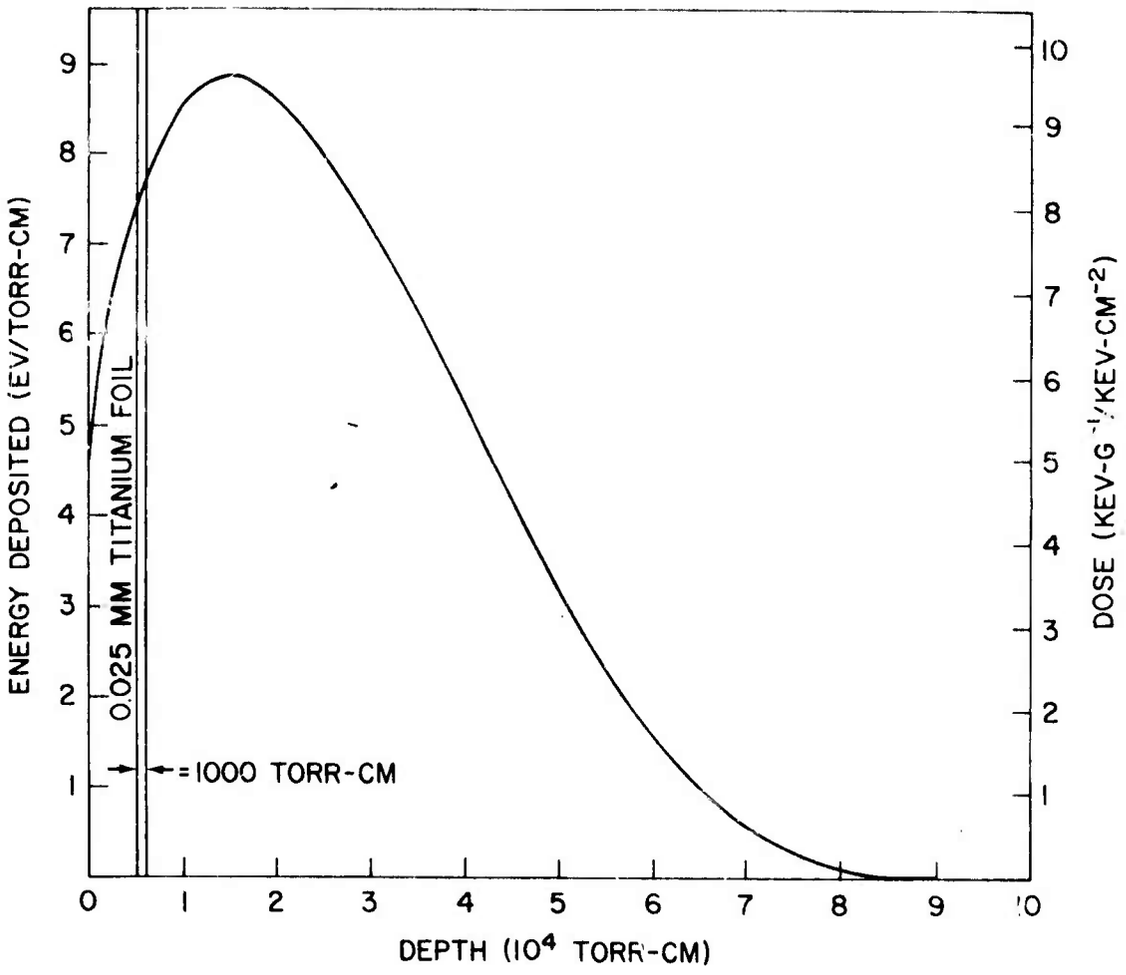

Fig. 2 - Energy deposition for 433 keV electrons in Ar. Fourteen percent of the total energy is absorbed by the 25-micron Ti foil whose scattering properties substantially increase the low pressure gas dose. The closely spaced parallel lines show the small absorption due to 1000 torr-cm of Ar.

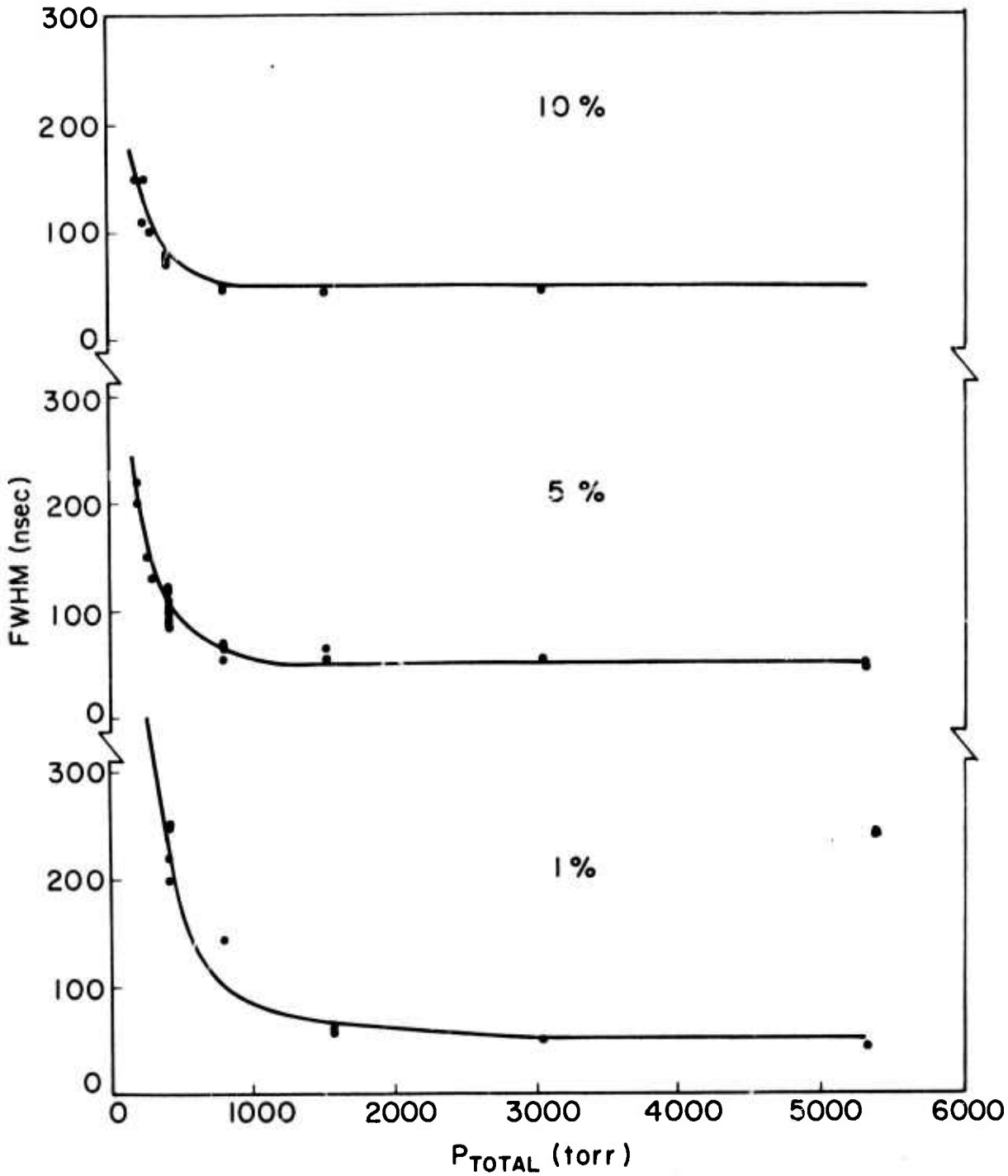

Fig. 3 - FWHM of N_2(C-B) fluorescence arising from a 50-ns long e-beam excitation of Ar with 1%, 5%, and 10% N_2. The solid line is theoretical while the dots are experimental.

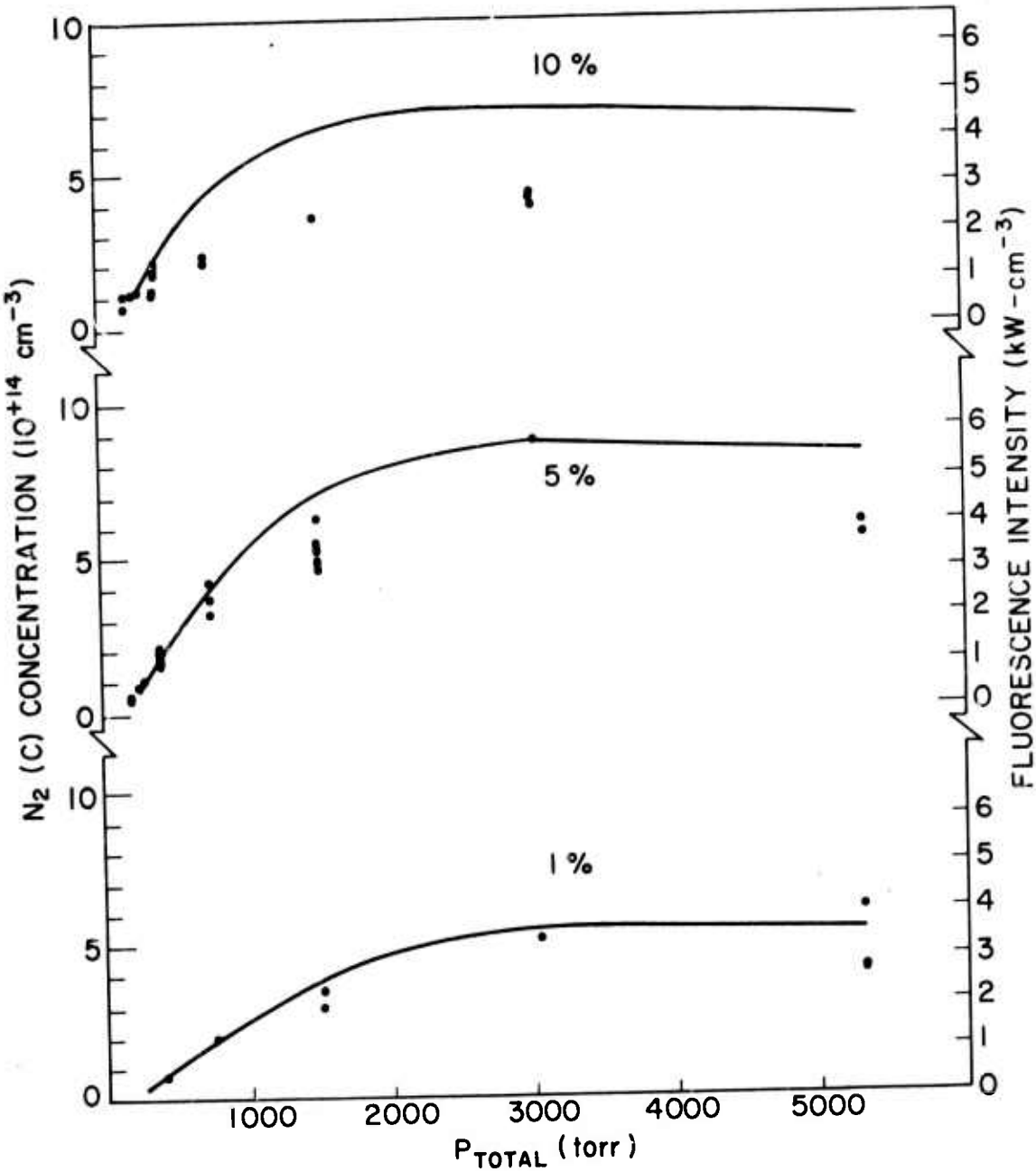

Fig. 4 - Peak $N_2(C)$ concentration as a function of the total pressure of Ar with 1%, 5%, and 10% N_2. The solid line is theoretical while the dots are experimental.

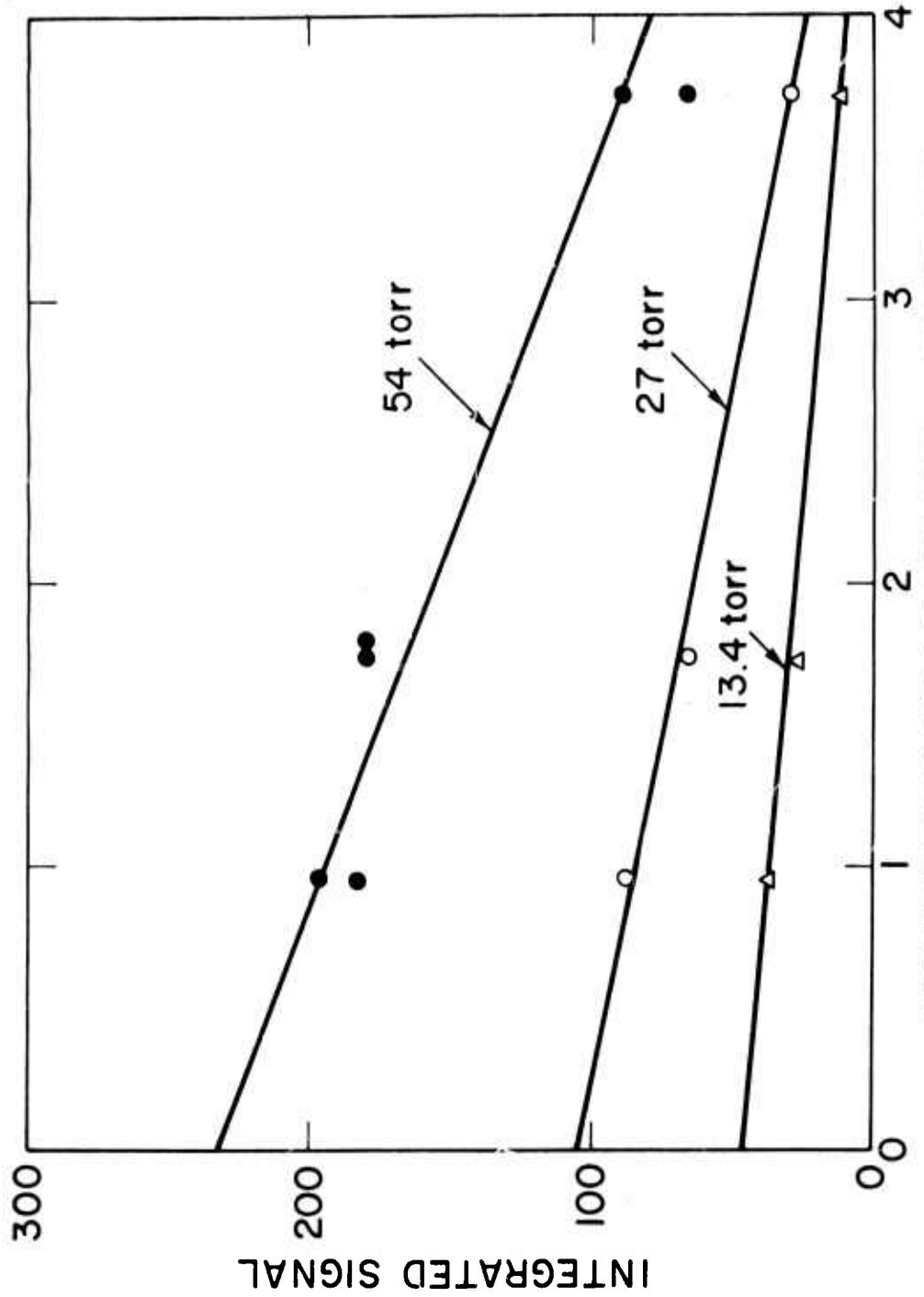

Fig. 5 - Integrated photodiode signal plotted versus percentage Br_2 according to the total pressure. The units along the ordinate result from the direct integration of the oscillographic traces (volts-time) taken with a 25-Ω line on a nanosecond time scale.

TABLE I

MECHANISMS FOR E-BEAM PRODUCTION OF ELECTRONICALLY EXCITED STATES

A. The $Ar-N_2$ System

STEP		k^a	REFERENCE
1.	$Ar^+ + 2Ar \rightarrow Ar_2^+ + Ar$	2.5×10^{-31}	b
2.	$Ar_2^+ + e \rightarrow Ar^* + Ar$	7×10^{-7}	c
3.	$Ar^* + 2Ar \rightarrow Ar_2^* + Ar$	6×10^{-33}	d
4.	$Ar^* + N_2 \rightarrow N_2(C) + Ar$	6×10^{-12}	e
5.	$Ar^* + N_2 \rightarrow$ all products	3×10^{-11g}	d
6.	$N_2(C) + Ar \rightarrow N_2 + Ar$	3×10^{-13}	f
7.	$N_2(C) \rightarrow N_2(B) + h\nu$	2.5×10^{7}	g
8.	$N_2(C) + N_2 \rightarrow 2N_2$	1.15×10^{-11}	h

B. The $Xe-Br_2$ System

9. $Xe^+ + 2Xe \rightarrow Xe_2^+ + Xe$
10. $Xe_2^+ + e \rightarrow Xe^* + Xe$
11. $Xe^* + Br_2 \rightarrow XeBr^* + Br$
12. $Xe^* + Br_2 \rightarrow$ all products
13. $XeBr^* \rightarrow Xe + Br + h\nu$

a. Radiative units, sec^{-1}; two-body units, cm^3/sec; and three-body units, cm^6/sec.

b. E. W. McDaniel, V. Cermak, A. Dalgarno, E. E. Ferguson, L. Friedman, Ion-Molecule Reactions (Wiley-Interscience, New York, 1970), p. 338.

c. J. N. Bardsley and M. A. Biondi, in Advances in Atomic and Molecular Physics (Academic, New York, 1970), Chap. I.

d. J. LeCalvé and M. Bourène, J. Chem. Phys. 58, 1446 (1973).

e. This work.

f. D. W. Setser, D. H. Stedman and J. A. Coxon, J. Chem. Phys. 53, 1004 (1970).

g. A. W. Johnson and R. G. Fowler, J. Chem. Phys. 53, 65 (1970).

h. P. Millet, Y. Salamero, H. Brunet, J. Galy, D. Blanc and J. L. Teyssier, J. Chem. Phys. 58, 5839 (1973).

References

1. S. K. Searles and G. A. Hart, Appl. Phys. Lett. 25, 79 (1974).

2. G. A. Hart and S. K. Searles, to be published.

3. S. K. Searles and G. A. Hart, Appl. Phys. Lett. 27, 243 (1975).

4. R. G. Little and M. B. Kime, IEEE Trans. Nucl. Sci. NS-20, 645 (1973).

5. ARPA-NRL Laser Program Semiannual Technical Report (December 1974).

6. D. B. Brown, D. B. Wittry, and D. F. Kyser, J. Appl. Phys. 40, 1627 (1969).

7. L. G. Christophorou, Atomic and Molecular Radiation Physics, Wiley-Interscience, N. Y. (1971) p. 35.

8. L. R. Peterson and J. E. Allen, Jr., J. Chem. Phys. 56, 6068 (1972).

9. C. E. Treanor, Math. Compt. 20, 39 (1966).

10. D. W. Setser, D. H. Stedman, and J. A. Coxon, J. Chem. Phys. 53, 1004 (1970).

11. R. M. Hill, R. A. Gutcheck, D. L. Huestis, D. Mukherjee and D. C. Lorents, Stanford Research Institute Report No. MP 74-39 (July 31, 1974).

APPENDIX C

KINETIC MODEL OF THE XeBr RARE GAS MONOHALIDE EXCIMER LASER*

G. A. Hart+ and S. K. Searles

Abstract

A kinetic model of the XeBr rare gas monohalide excimer laser is presented. Agreement of predicted and observed side emission from low pressure Xe:Br_2 mixtures was used to determine rate constants for the formation of XeBr* from Xe* and Br_2 ($2.0 \pm 0.4 \times 10^{-9}$ cm^3/sec) and the quenching of XeBr* by Br_2 ($8 \pm 2 \times 10^{-10}$ cm^3/sec), as well as the radiative lifetime of XeBr* (17.5 ± 2.5 ns).

* Work supported in part by DARPA.

+ NRC-NRL Postdoctoral Research Associate 1973 - Present.

The recent development [1-4] of efficient and powerful rare gas monohalide uv excimer lasers pumped by pulsed high-energy electron beam sources has created a strong need for kinetic models giving an accurate description of the mechanisms responsible for the fluorescence and laser emission observed from these systems. We wish to present a kinetic model for the first reported rare gas monohalide excimer laser, the XeBr system, and to report rate constants we have measured for the principal reactions in that model.

In a previous paper[1] a three-step mechanism for the kinetics of the XeBr laser was proposed together with a description of the apparatus used to conduct both the kinetics and laser emission studies. The three reactions of this model are given as steps 1-3 of Table I. In establishing this rather simple scheme as that responsible for the fluorescence and laser emission observed from XeBr* and in determining several key rate constants in this model which were previously unreported, possible alternate reactions involving the species of interest were considered. These are also presented in Table I together with the currently available rate constants for these processes.

Only one previous measurement of the reaction rate for step 2 had been reported[5], and that was for a flowing afterglow experiment where the identity of the excited Xe* species was known to be metastable $Xe(^3P_2)$ atoms. In an

earlier study of the rate of energy transfer from Ar* to N_2[6] it was found that because of the extremely complex chemical and electrical environment generated by a high current density relativistic e-beam it is advisable to determine the influence of such a dynamic environment on reaction rate constants measured under more stable conditions. In high energy e-beam experiments the identity of excited rare gas species such as Xe* is often not well known since energetic secondary electrons can maintain an equilibrium between the rare gas metastables and nearby non-metastable excited states. These neighboring excited states can exhibit significantly enhanced or inhibited reactivity with respect to a proposed laser pumping reaction[7]. In those cases where the reactivity of close-lying states is greater than that of the metastables the effective rate constant is proportionally increased depending on the admixture of excited rare gas states held in dynamic equilibrium by secondary electron collisions. It is such a collective rate constant that was to be determined for step 2 in this study. In addition, no value of the radiative lifetime of XeBr* had been reported, nor had the rate at which this excited species is quenched by Br_2 been determined. A knowledge of these three rates is essential for an understanding of the temporal behavior and energy output of the XeBr laser under various operating conditions. Before these important rate

constants could be measured, it was necessary to establish for what partial pressures of Xe and Br_2 this simple model would provide an accurate description of the production of XeBr*. By comparing various competitive energy pathways it was determined that for low relative concentrations of Br_2 and low total pressures steps 1-3 would be primarily responsible for the observed XeBr* fluorescence temporal behavior.

Under these conditions steps 4-11 in Table I can be regarded as negligible. The justification for this important assumption can be most clearly understood by considering the effective first order rate constants plotted in Figure 1. The reactive species initially present when a 100:1 $Xe:Br_2$ mixture is pulsed by a high energy e-beam are Xe*, Xe^+ and Br_2. By investigating the reaction channels available to each of these species the validity of regarding steps 4-11 as negligible can be verified. Figure 1 displays these relative reaction rates for Xe*, Xe^+ and Br_2 as well as XeBr* in 100:1 $Xe:Br_2$ mixtures at various pressures excited by the NRL 433 keV e-beam.

The only competitive reaction involving Xe* is the three body reaction of step 5 which yields Xe_2*. However, for the pressures at which kinetic data were taken, total pressure less than sixty torr, the dimerization of Xe* occurs at a rate roughly two orders of magnitude slower than that reported by Velazco and Setser[5] for the reaction of Xe*

and Br_2. Hence the production of Xe_2^* and its subsequent radiative decay or reaction with other species is totally negligible, leaving step 2 as the only reaction of consequence for Xe*.

Since the e-beam initially produces approximately three Xe^+ for each Xe* according to an extrapolation of the Peterson and Allen[8] results for argon to the case of xenon, the subsequent reactions involving Xe^+ could have a significant effect on the overall mechanism. However, a recent measurement of the rate constant for the charge transfer reaction between Xe^+ and Br_2[9] indicates that this process proceeds thirty times more slowly than step 2 and hence plays a secondary role. Dimerization of the Xe^+ ions occurs at a rate at least ten times slower than that of step 2. In addition our measurement of the reaction rate for step 2 produced a rate constant approximately four times larger than the previously reported value, confirming the validity of our assumption that Xe^+ plays no significant kinetic role under the conditions we investigated. The effective first order rate constant for Xe* due to reaction with Br_2 using our rate constant is also shown in Figure 1.

The previous arguments served to demonstrate that although both Xe* and Xe^+ are produced by the e-beam pulse and several possible subsequent reactions involving these species could be postulated, under the experimental conditions

selected for this kinetic study, step 2 is the dominant reaction and all others can be neglected. This assertion is further strengthened by considering that as a consequence of the negligible concentrations of Xe_2^* and Xe_2^+ present at low xenon partial pressures, the only three species which Br_2 might react with are Xe^*, Xe^+, and e^-. As is shown in Figure 1 the effective first order rate constant for the reaction of Br_2 with Xe^* is at least an order of magnitude greater than that for the competing reactions with Xe^+ and e^-. This comparison was made with the previously reported rate constant for step 2, and hence an even more favorable comparison could be made using the value we obtained for this reaction rate.

To make this comparison an estimate of the populations of Xe^*, Xe^+, and e^- produced by the initial e-beam pulse is necessary. The energy deposition of the relativistic e-beam was calculated using the TEP computer code[10,11]. This code predicts a dose for 433 keV electrons passing through xenon at 300°K of 0.0512 joules deposited per cm-atm for each joule incident. The corresponding value from a simple Berger and Seltzer[12] stopping power calculation would be 0.0156 $J\text{-}cm^{-1}\text{-}atm^{-1}/J$. The factor of three difference in dose rate is primarily due to multiple scattering in the xenon as well as in the adjacent 37.5-μ-thick Inconel 750-X foil and stainless steel cell walls. Using the TEP-predicted

dose, the experimental W value of 21.9 eV for xenon[13], and the aforementioned extrapolation of the Peterson and Allen[7] cross sections for argon to xenon, it can be calculated that the calorimetrically determined incident energy flux value of 2.52 J/cm^2 produces a total Xe^+ yield of 3.76×10^{16} cm^{-3} and a total Xe* yield of 1.24×10^{16} cm^{-3} for a xenon partial pressure of 1 atm.

Since kinetic data available prior to our study indicated that under the low pressures to be investigated the clearly predominant reaction would be that given in step 2, the fluorescence predicted by a model consisting of steps 1-3 was compared to side emission data taken at a set of mixture compositions and total pressures. Fluorescence from $Xe:Br_2$ mixtures of 27.1, 57:1, and 106:1 at 13.4, 27 and 54 torr was monitored by an ITT F-4018-S5 photodiode.

Because the decay portions of the fluorescence oscillographs so obtained are a function of both the XeBr* lifetime and rate of production, with neither serving as a predominant rate-determining step, it is impossible to employ a simple procedure such as extracting a 1/e decay time and then relate the result to an individual process. It was also determined that merely fitting the predicted fluorescence FWHM and time to peak emission to the observed fluorescence curves was a far less sensitive test of various lifetime rate constant pairs than is achieved by comparing

the shape of the observed and predicted fluorescence on a point by point basis. Consequently the oscillograph data was digitized and a best least-squares fit was obtained between the observed fluorescence and the three step model by varying the step 2 rate constant and XeBr* lifetime. As can be seen in Figure 2 the predicted fluorescence decay is much more sensitive to the parameters used than is the rising portion of the fluorescence curve. To exploit this behavior twenty-one equally spaced points along the fluorescence decay portion of each oscillograph were digitized. The spacing for a given trace was determined by the time required for the fluorescence to fall from its peak to roughly 5% of its maximum value. This duration was divided into twenty segments. The relative intensities so obtained were used as input data to a Runge-Kutta numerical integration of steps 1-3 which calculated XeBr* populations as a function of time. This numerical method was used rather than the alternative of integrating the simple differential equations of steps 1-3 because the trapezoidal shape of the Xe* source term resulted in an algebraically cumbersome analytical expression which offered no advantage in terms of providing a straightforward method of determining the desired rate constants. In addition the Runge-Kutta routine could be far more readily modified to include the effect of Br_2 quenching or other processes which become important

at higher partial pressures. It should be noted that although the shape of the predicted fluorescence curves for this three-step model is dependent on the shape of the source term for Xe*, as determined by the e-beam current pulse, it is independent of the intensity of that term. Thus the kinetic data obtained is not dependent on the accuracy of the computer code used to predict e-beam energy deposition.

Figure 2 shows the close agreement achieved between the kinetic model and the observed fluorescence for one set of experimental conditions. The XeBr* formation rate constant of 2×10^{-9} cm^3/sec and XeBr* lifetime of 17.5 ns was found to produce the overall best agreement across the range of pressures and compositions investigated. These values correspond to the distinct minimum standard deviation shown in Figure 3 which summarizes the agreement for all the cases considered.

As was discussed in a previous paper[1], the fact that the XeBr* fluorescence intensity was inversely proportional to the Br_2 concentration for high partial pressures of Br_2 indicated that Br_2 was quenching XeBr*. By adding the quenching reaction given in step 4 of Table I to the kinetic model even better agreement was achieved between predicted and observed fluorescence, partially for the 54 torr 27:1 $Xe:Br_2$ mixture. In this way a quenching rate constant of 8×10^{-10} cm^3/sec for step 4 was determined. The

resulting effective first order rate constant due to such quenching in a 1% Br_2 mixture is also plotted in Figure 1 together with the reciprocal of the measured lifetime. No corresponding quenching of XeBr* due to xenon was observed when the Br_2 partial pressure was held constant and the total pressure was increased.

In conclusion, a comparison of the previously reported rate for the reaction of Xe* + Br_2 to form XeBr* with currently available rates for other possible processes in Xe:Br_2 mixtures excited by a high energy e-beam indicated that for low Xe and Br_2 partial pressures the direct reaction of Xe* and Br_2 is primarily responsible for the formation of XeBr*. Data collected under these conditions provided a new value for the rate constant of this reaction together with the first measurement of the radiative lifetime of XeBr*. By increasing the partial pressure of Br_2 the rate constant for the quenching of XeBr* by Br_2 was determined. Besides being of fundamental interest in obtaining a better understanding of this new class of excimers, these three rates establish the conditions under which it is possible to observe laser action in such mixtures. In a subsequent paper the observed temporal behavior and energy output of the XeBr* laser will be discussed in terms of these key rates.

TABLE I

MECHANISM FOR POPULATION OF XeBr*

	STEP	k^a	REFERENCE
1.	$\vec{e} + Xe \rightarrow Xe^* + \vec{e}$ $Xe^+ + \vec{e} + e$	b	c,d, e,f
2.	$Xe^* + Br_2 \rightarrow XeBr^* + Br$	4.63×10^{-10} $2.0 \pm 0.4 \times 10^{-9}$	g h
3.	$XeBr^* \rightarrow Xe + Br + h\nu(281.8\ nm)$	5.71×10^{7}	h
4.	$XeBr^* + Br_2 \rightarrow Xe + Br + Br_2$	$8 \pm 2 \times 10^{-10}$	h
5.	$Xe^* + 2Xe \rightarrow Xe_2^* + Xe$	5×10^{-32}	d
6.	$Xe_2^* \rightarrow 2Xe + h\nu$	2×10^{8}, 2.5×10^{7}	e
7.	$Xe^+ + Br_2 \rightarrow Br_2^+ + Xe$	1.5×10^{-11}	i
8.	$Xe^+ + 2Xe \rightarrow Xe_2^+ + Xe$	2.5×10^{-31}	d
9.	$Xe_2^+ + e^- \rightarrow Xe^* + Xe$	2×10^{-7}	d
10.	$Xe_2^+ + Br_2 \rightarrow Br_2^+ + 2Xe$	j	
11.	$Br_2 + e^- \rightarrow Br^- + Br$	8.2×10^{-13}, 296°K 8.2×10^{-12}, 2.8 eV	k

---

a Radiative units, sec^{-1}; two-body units, cm^3/sec; and three-body units, cm^6/sec.

b W = 21.9 eV/ion pair. Ratio Xe^+/Xe^* determined by method used for Ar^+/Ar^* ratio is 3.04/1.

c Reference 12

d D. C. Lorents, D. J. Eckstrom and D. Huestis, Stanford Research Institute Report #MP73-2, 1973 (unpublished).

e E. V. George and C. K. Rhodes, Appl. Phys. Lett. 23, 139 (1973) and C. W. Werner, E. V. George, P. W. Hoff and C. K. Rhodes, Appl. Phys. Lett. 25, 235 (1974).

f Reference 7.

g Reference 5

h This work

i Reference 8

j ΔE = -0.6, -1.37 eV

k F. K. Truby, Phys. Rev. A4, 613 (1971).

References

1. S. K. Searles and G. A. Hart, Appl. Phys. Lett. 27, 243 (1975).
2. J. J. Ewing and C. A. Brau (private communication).
3. M. L. Bhaumik (private communication).
4. A. K. Hays, G. C. Tisone, and J. M. Hoffman (private communication).
5. J. E. Velazco and D. W. Setser, J. Chem. Phys. 62, 1990 (1975).
6. S. K. Searles and G. A. Hart, Appl. Phys. Lett. 25, 79 (1974).
7. D. H. Stedman and D. W. Setser, Chemical Applications of Metastable Rare Gas Atoms, (Pergamon Press, New York, 1971), p. 219.
8. L. R. Peterson and J. E. Allen, Jr., J. Chem. Phys. 56, 6068 (1972).
9. S. Lias and P. Ausloos (private communication).
10. D. B. Brown, D. B. Wittry, and D. F. Kyser, J. Appl. Phys. 40, 1627 (1969).
11. G. A. Hart and S. K. Searles, ARPA-NRL Laser Program Semiannual Technical Report to Defense Advanced Research Projects Agency, 1 July 1974 - 31 December 1974, p. 64.
12. M. J. Berger and S. M. Seltzer, in Studies in Penetration of Charged Particles in Matter, Nuclear Science Series Report No. 10, NAS-NRC Pub. 1133 (National Academy of Sciences, Washington, 1964).

13. L. G. Christophorou, Atomic and Molecular Radiation Physics, (Wiley-Interscience, New York, 1971), p. 35.

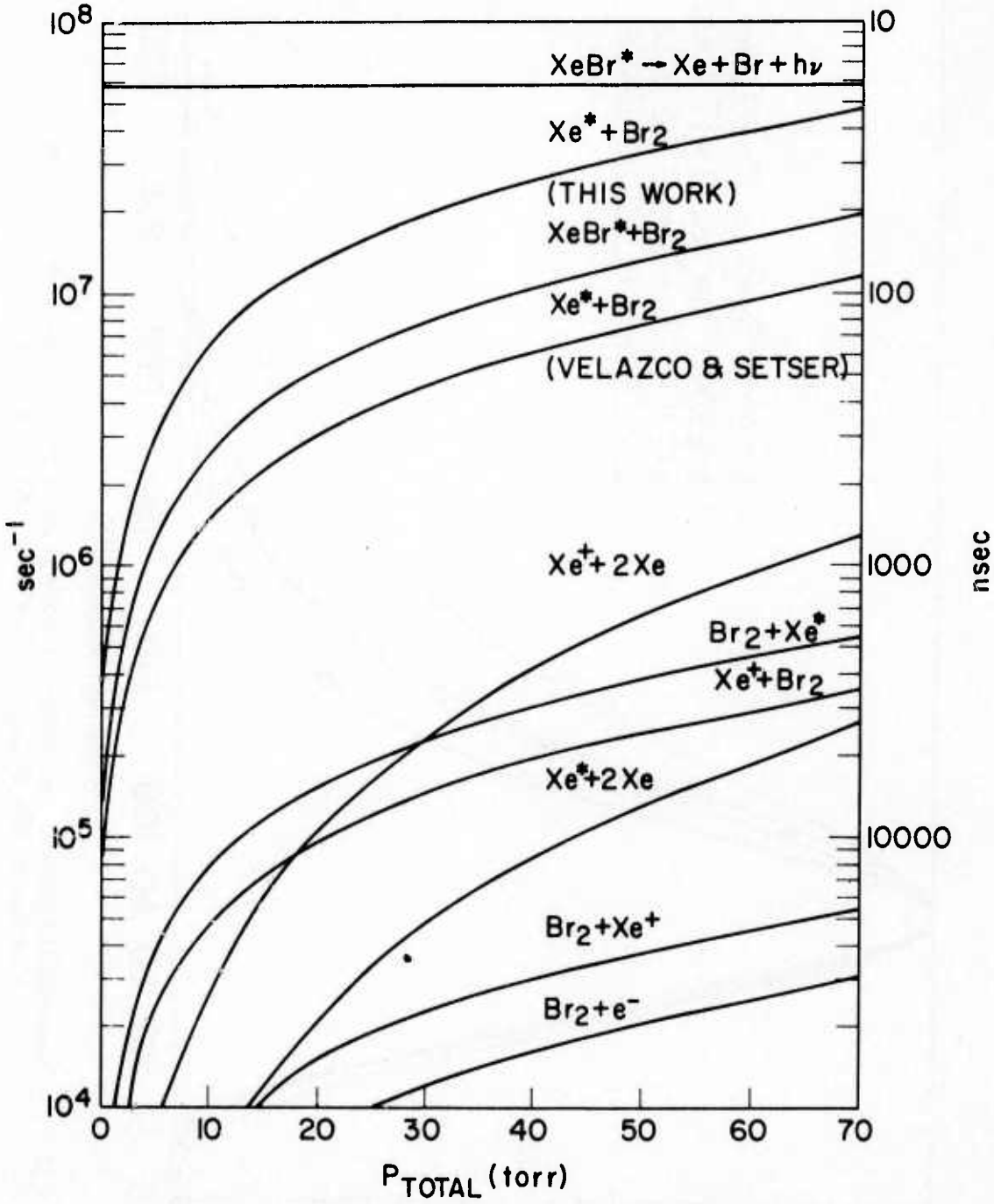

Fig. 1 - Effective first order rate constants for reactions in 100:1 Xe:Br_2 mixtures

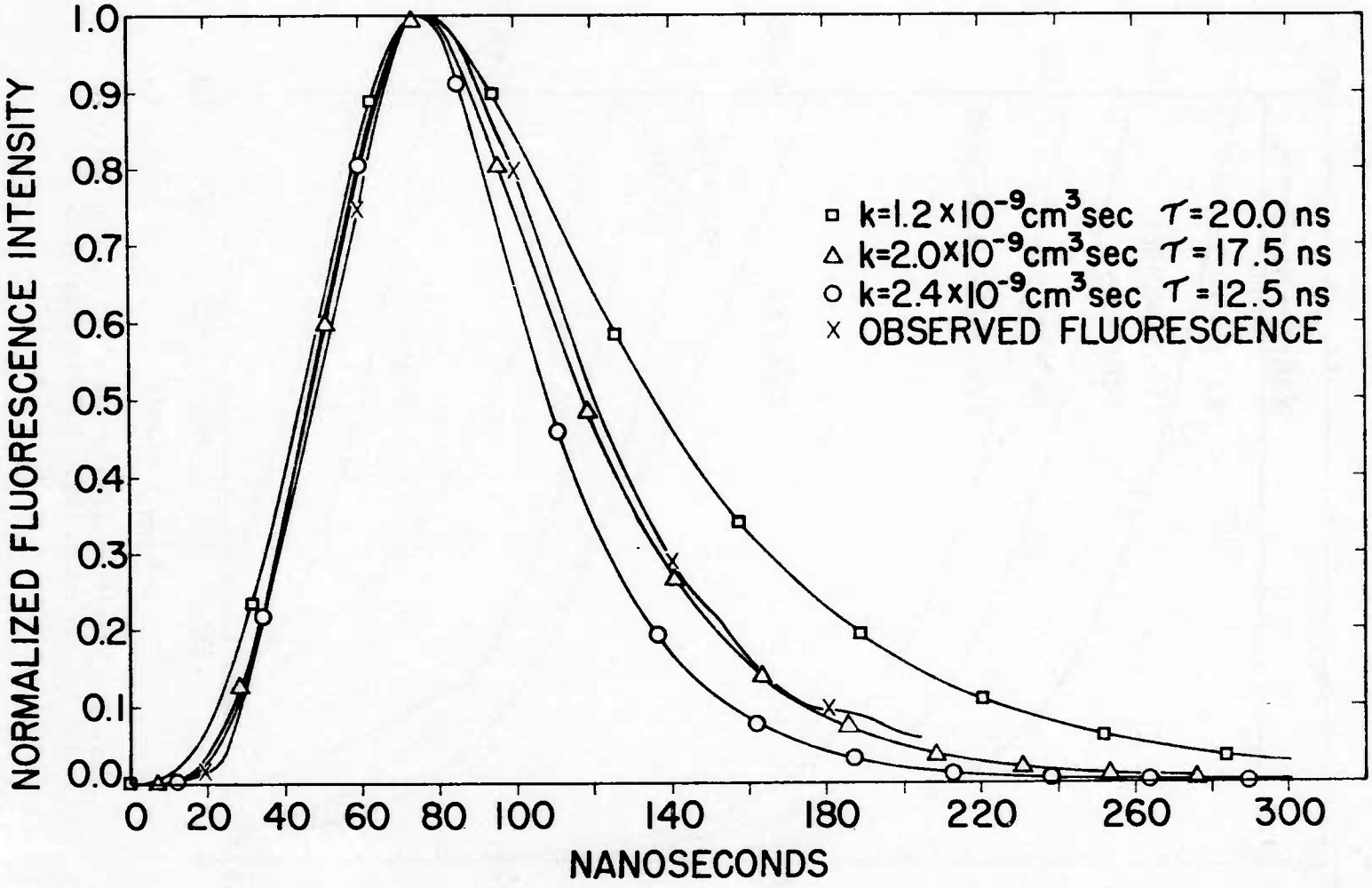

Fig. 2 - Temporal behavior of XeBr* fluorescence compared with three-step kinetic model P_{total} = 13.4 torr, Xe:Br_2 = 27:1

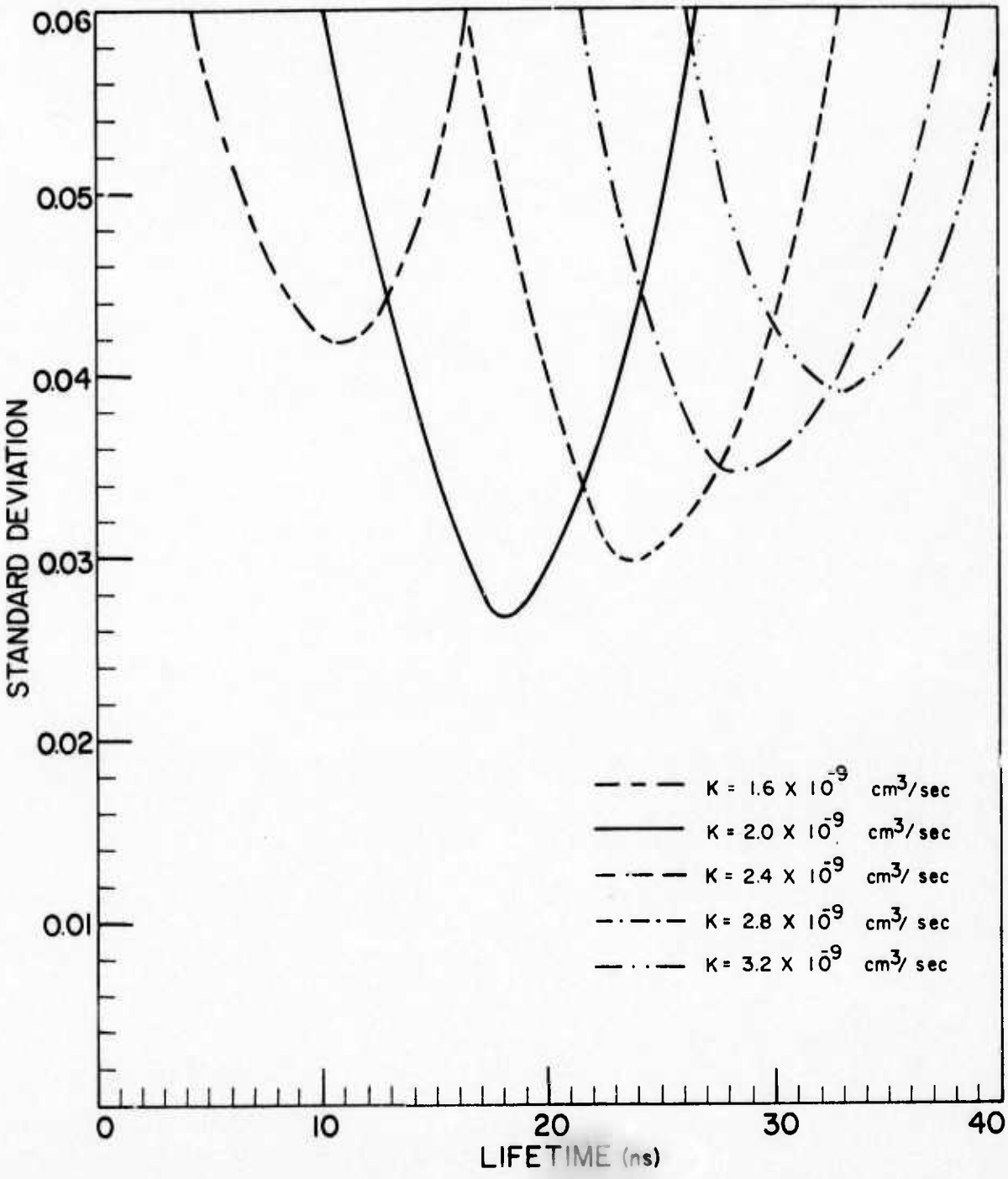

Fig. 3 - Agreement between three-step kinetic model and observed XeBr* fluorescence as a function of XeBr* production rate constant and radiative lifetime